Integrated Localization and Communication for IRS-Assisted Multi-User mmWave MIMO Systems

Xingyu Peng, *Graduate Student Member, IEEE*, Xiaoling Hu, *Member, IEEE*, Jiabao Gao, Richeng Jin, *Member, IEEE*, Xiaoming Chen, *Senior Member, IEEE*, and Caijun Zhong, *Senior Member, IEEE*

***Abstract*— This paper delves into the potential of intelligent reflecting surfaces (IRSs) in enabling integrated sensing and communication (ISAC) in multi-user multi-path scenarios. We introduce a three-dimensional (3D) multi-user ISAC framework with distributed IRSs, which offers simultaneous signal demodulation, channel estimation, and localization. The transmission is divided into a user access stage and a downlink transmission stage. In the first stage, we propose an algorithm for simultaneous uplink signal demodulation and angles of arrival (AoA) estimation at the semi-passive IRS. Moreover, a joint active and passive beamforming scheme inspired by radar-communication, is proposed to enhance both communication and localization performance in the downlink stage, while eliminating the need for distinct localization reference signals. Numerical results demonstrate that the proposed ISAC framework achieves centimeter-level localization accuracy while maintaining comparable communication performance to communication-only systems, thus validating its effectiveness.**

***Index Terms*— Intelligent reflecting surface (IRS), integrated sensing and communication (ISAC), beamforming, localization.**

I. Introduction

FUTURE communication systems are expected to support various advanced applications and services, such as machine-type communication, intelligent robotics, autonomous driving, virtual reality, and extended reality [1]. These emerging services and applications necessitate high-rate data transmission and high-accuracy sensing. However, the current approach of designing communication and sensing systems separately is inadequate in meeting these two requirements simultaneously. Moreover, high-rate data transmission and high-accuracy sensing impose severe demands on signal bandwidth, making the scarce spectrum more precious. To tackle this issue, researchers have explored the possibility of enabling simultaneous communication and sensing over the same spectrum. Resource allocation and interference coordination have been attempted to manage and minimize mutual interference between these systems [2], [3], [4]. However, this approach also leads to increased pilot overhead and requires strigent synchronization, ultimately hindering the overall spectrum efficiency of the system.

Fortunately, due to the wide deployment of the millimeter wave (mmWave) and massive multiple-input multiple-output (MIMO) technologies, communication signals in future wireless systems are expected to have high-resolution in both the time domain and the angular domain, which makes it possible to achieve high-precision sensing. Motivated by this, the study on integrated sensing and communication (ISAC) technology is quickly gaining research attention [9]. ISAC can be categorized into two categories according to the integration of sensing and communication waveform: radar-communication coexistence (RCC) and dual-functional radar-communication (DFRC). In RCC systems, although radar and communication functionalities share the same spectrum, they operate independently with distinct waveforms, necessitating meticulous interference management [5]. On the other hand, DFRC systems achieve a harmonious integration by employing the same waveforms for both sensing and communication, thus eliminating interference issues and enabling the concurrent execution of both functions on a single device [6].

However, the molecular absorption in the mmWave band is severe and the mmWave waves with strong directivity and poor diffraction are blocked by many obstacles more easily. To tackle these challenges, intelligent reflecting surfaces (IRSs) have gained substantial research interests from both acadima and industry due to its low cost, ease of deployment, and high spectrum efficiency [7]. IRS comprises a myriad of passive or semi-passive reflecting elements, and each reflecting element can independently adjust the phase or amplitude of the incident signal, thus exploiting the scattered signal in the wireless communication environment. On the one hand, the passive beamforming at IRS can realize better ISAC performance, on the other hand, IRS can provide a virtual line-

Manuscript received 18 June 2023; revised 24 November 2023 and 27 January 2024; accepted 7 March 2024. Date of publication 20 March 2024; date of current version 16 August 2024. This work was supported in part by the Zhejiang Provincial Natural Science Foundation of China under Grant LD21F010001, and in part by the Natural Science Foundation of China under Grant 62231009 and 62201084. An earlier version of this paper was presented in part at the IEEE Wireless Communications and Networking Conference (WCNC), Dubai, United Arab Emirates, April 2024. The associate editor coordinating the review of this article and approving it for publication was B. Smida. *(Corresponding author: Richeng Jin.)*

Xingyu Peng, Jiabao Gao, Richeng Jin, Xiaoming Chen, and Caijun Zhong are with the College of Information Science and Electronic Engineering, Zhejiang University, Hangzhou 310027, China, and also with the Zhejiang Provincial Key Lab of Information Processing, Communication, and Networking (IPCAN), Hangzhou China, 310007 (e-mail: peng_xingyu@zju.edu.cn; gao_jiabao@zju.edu.cn; richengjin@zju.edu.cn; chen_xiaoming@zju.edu.cn; caijunzhong@zju.edu.cn).

Xiaoling Hu is with the State Key Laboratory of Networking and Switching Technology, Beijing University of Posts and Telecommunications, Beijing 100876, China (e-mail: xiaolinghu@bupt.edu.cn).

Color versions of one or more figures in this article are available at https://doi.org/10.1109/TCOMM.2024.3379399.

Digital Object Identifier 10.1109/TCOMM.2024.3379399

of-sight (V-LoS) path between the BS and the users. Therefore, we focus on the IRS-assisted ISAC systems in this paper. And the related works are summarized in the following to motivate our contributions.

A. Related Work

Effective transmit beamforming design is the key to unlocking the potential of ISAC systems. Motivated by this, many works have studied beamforming design in ISAC systems to enhance both communication and sensing performance [8], [9], [10], [11]. Specifically, the work [9] proposed a beamforming algorithm for the dual-functional MIMO radar-communication system, where the base station (BS) enables joint radar sensing and multi-user communications, simultaneously. The work [10] took the Pareto boundary of the achievable Cramer-Rao bound-rate (C-R) region as the performance metric to design the transmit covariance matrix, enabling the joint sensing of point/extended targets and communication with the users. Besides, work [11] proposed a code-division scheme for the OFDM ISAC systems to make sure that communication and sensing do not interfere with each other.

IRS-aided communication systems have garnered significant attention in recent years. Specifically, the implementation of an IRS with M reflecting elements allows for a power gain of M^2, as demonstrated in [12]. In [13], the authors employed a cooperative approach by combining active and passive IRSs to establish a virtual LoS multi-reflection path from the BS to the user, which outperforms single IRS systems. The combination of IRS and unmanned aerial vehicles (UAVs) was explored in [14] and [15], which validates the capability of IRS to enhance spectrum and energy efficiency.

IRS has also been adopted to enhance ISAC performance, spectrum efficiency, as well as sensing coverage range due to the additional V-LoS paths. An IRS-assisted ISAC system was considered in work [16], where a scheme for joint active beamforming and passive beamforming was designed by maximizing the worst-case target illumination power while guaranteeing the signal-to-interference-plus-noise ratio (SINR) for each user, thus directly improving the communication and the sensing performance compared with the ISAC system without IRS. The potential of IRS in supporting target detection was explored in [17], where the detection probability was derived in closed-form, and the beamforming scheme was designed by maximizing the received power at the user, while ensuring a lower bound on detection probability constraint. Non-orthogonal multiple access was considered in [18], which enabled joint communication and sensing through the optimization of beamforming and power allocation. In [19], the authors considered cross-correlation patterns for serving communication users and tracking targets. Two cases were presented depending on whether interference between the IRS and the radar-communication BS was taken into account, where beamforming schemes were designed. Furthermore, the work [20] investigated the security problem in the ISAC systems for preventing information leakage, and leveraged IRS to create a virtual link for target sensing and preventing eavesdropping.

However, all the above works assume perfect channel state information (CSI), which comes at the cost of prohibitive pilot overhead. Practical systems suffer from CSI errors caused by noise, limited training or imprecise CSI feedback [47]. Therefore, it is essential to take imperfect CSI into consideration in the ISAC systems. Besides, the sensing performance metrics considered in the aforementioned works is either Cramer-Rao bound (CRB) or beampattern gain, which cannot directly capture the velocity, driving direction, acceleration, and location information of the target. Despite some recent works, such as [22] and [23], achieving users location estimation in the IRS-aided ISAC system, they fail to consider the significant impact of non-line-of-sight (NLoS) paths and multi-user interference.

B. Contributions

To address the shortcomings of prior works, in this work, the imperfect CSI, NLoS paths and multi-user interference are taken into consideration. In the presence of NLoS, it is challenging to directly acquire the angle information corresponding to LoS path due to the uncertain locations of the scatterers and the impact of IRS on incident signals. Furthermore, concurrent location sensing, signal demodulation, and channel estimation are incorporated. To the best of our knowledge, this is the first work that tackles the challenges of simultaneously localizing multiple users, estimating the channels, and demodulating the transmit signals while accounting for NLoS paths under imperfect CSI. The main contributions are summarized as follows:

- We propose a novel ISAC framework for the distributed semi-passive IRS-assisted 3D multi-user MIMO system, which incorporates transmission protocols, beamforming design schemes, channel estimation methods, and user localization algorithms, to enable concurrent channel estimation, signal demodulation, and user localization.
- We propose a radar-inspired beamforming scheme by minimizing the maximum the weighted cross-correlation and auto-correlation beampattern gain among the users based on partial angle information estimated by semi-passive IRSs, endeavoring to enhance both downlink communication and localization performance.
- Unlike traditional communication systems where channel estimation and signal demodulation are performed separately, we design a semi-blind two-stage algorithm that utilizes the statistical characteristics of transmit data to simultaneously perform both tasks with reduced pilot overhead. Simulation results imply that the proposed two-stage algorithm outperforms existing methods in terms of channel estimation accuracy and achieves demodulation performance comparable to the minimum mean square error (MMSE) method with perfect CSI.
- We consider a more practical geometric channel model that incorporates numerous NLoS paths, in contrast to traditional IRS-assisted localization systems that focus solely on line-of-sight (LoS) path. To address this, we propose an effective path separation algorithm based on the statistical characteristics of transmit data, which

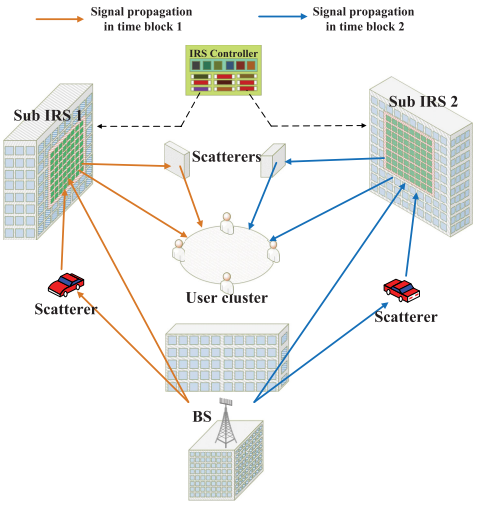

Fig. 1. System model: An IRS assisted ISAC system.

ensures precise estimation of the angle of the LoS path. Consequently, our method achieves comparable user localization accuracy to existing methods that utilize dedicated positioning reference signals.

The remainder of the paper is organized as follows. Section II introduces the distributed IRS-assisted ISAC system and the proposed integrated communication and localization (I-CALL) framework. The user access stage is designed in Section III, while the downlink transmission stage is designed in Section IV. Numerical results and discussions are provided in Section VI, and finally, Section VII concludes the paper.

II. System Model

We consider an IRS-assisted ISAC multi-user mmWave system, as illustrated in Fig. 1, where one BS with N_B element uniform linear array (ULA) along the y-axis, communicates with K users each with an $N_U = N_{ux} \times N_{uy}$ uniform rectangular array (URA) lying on the x-y plane. The paths between the BS and the users are obstructed as in [22] and [23], and a distributed semi-passive IRS[1] is deployed to establish VLoS reflection paths and assist user localization and communication. Specifically, the semi-passive IRS consists of two sub-IRSs,[2] both have $M = M_y \times M_z$ URA lying on the y-z plane and contain M_a semi-passive reflecting elements. Besides, a backhaul link connects the BS and the two sub-IRSs for information exchange, and both the user-IRS and the IRS-BS channels are modeled as quasi-static block-fading channels [16], which remain almost unchanged during each coherence block but vary from one block to another.

[1]The concept of semi-passive Intelligent Reflecting Surfaces (IRS) was introduced in previous studies [12], [24], [25]. It integrates a small number of radio frequency (RF) chains into the IRS, enabling selected reflecting elements to perform signal processing tasks for channel and parameter estimation with low power consumption.

[2]According to the principle of localization [49], it is imperative to employ two IRSs to offer enough degrees of freedom in the spatial domain and gather precise location information without introducing additional priori information, such as time of arrival (TOA)/time of difference arrival (TDOA) [50], and received signal strength (RSS) [51].

A. Two-Stage Transmission Protocol

The proposed transmission protocol for the I-CALL framework is illustrated in Fig. 2. We consider the transmission period within one coherence block that comprises two stages, i.e., the user access stage with τ_0 time slots and the downlink transmission stage with T_0 time slots.

1) User Access Stage: In the first stage, we roughly estimate the angles of arrival (AoAs) at sub-IRSs within a short period[3] based on the received signals, endeavoring to enhance the communication and localization performance in the second stage by carrying out a beamforming scheme. Specifically, during the user access stage, the users transmit pilot symbols with $\tau_{0,\mathrm{p}}$ time slots and data symbols with $\tau_{0,d}$ time slots. The two semi-passive sub-IRSs turn on all the semi-passive reflecting elements and operate in the sensing mode to carry out the effective AoA estimation task, which is then sent to the BS via the backhaul link.

2) Downlink Transmission Stage: During the downlink transmission stage, each user simultaneously estimate the transmit data, and the effective AoAs at users by exploiting the statistical characteristics of the received signals. Based on this, the users then reconstruct the channels by pairing all the estimated AOAs with their associated paths. Then, combining the angular information of LoS path, the location of the users can be estimated. Specifically, the BS first carries out the beamforming optimization task by using the estimated effective AoAs in the first stage. Then, it sends short pilot symbols[4] with τ_1 time slots and data symbols with τ_2 time slots to all the users. The downlink transmission stage is divided into two time blocks with T_1 and T_2 time slots. During each time block, one sub-IRS works under the reflecting mode with the other sub-IRS being switched off.[5]

B. Transmission Model

In this subsection, we will introduce the signal received in both the user access stage and the downlink transmission stage.

1) User Access Stage: During the user access stage, the symbols transmitted by the k-th user are denoted by $\mathbf{s}_{\mathrm{u},k} = [\mathbf{s}^{\mathrm{p}}_{\mathrm{u},k}, \mathbf{s}^{\mathrm{q}}_{\mathrm{u},k}] \in \mathbb{C}^{1\times\tau_0}$, where $\mathbf{s}^{\mathrm{p}}_{\mathrm{u},k} = [s_{\mathrm{u},k}(1), \cdots, s_{\mathrm{u},k}(\tau_{0,\mathrm{p}})]$ and $\mathbf{s}^{\mathrm{q}}_{\mathrm{u},k} = [s_{\mathrm{u},k}(\tau_{0,\mathrm{p}+1}), \cdots, s_{\mathrm{u},k}(\tau_0)]$ denote the pilot symbols and the data symbols, respectively, and $s_{u,k}(t)$ is the symbol transmitted at time slot $t \in \mathcal{T}_{\mathrm{u}} = \{1, \cdots, \tau_{0,\mathrm{p}}, \cdots, \tau_0\}$. Two semi-passive sub-IRSs operate in the sensing mode, and the received signal at the j-th sub-IRSs in time slot $t \in \mathcal{T}_{\mathrm{u}}$ is

$$\mathbf{y}_{\mathrm{u},j}(t) = \sum_{k=1}^{K} \sqrt{P_{\mathrm{u}}}\mathbf{H}_{\mathrm{U2I},j,k}\mathbf{w}_{\mathrm{u},k}s_{\mathrm{u},k}(t) + \mathbf{n}_{\mathrm{u}}(t), j = 1, 2, \tag{1}$$

[3]The proposed transmission model reduces the duration of the user access stage while increasing the duration of the downlink transmission stage. This approach helps mitigate the impact of semi-passive reflecting elements on overall system performance.

[4]By exploiting the statistical characteristics of the received signals, the number of pilot symbols needed for channel estimation can be reduced.

[5]This paper aims to demonstrate a new modular workflow under ISAC systems, and the algorithms in each stage are not limited to those proposed in this paper.

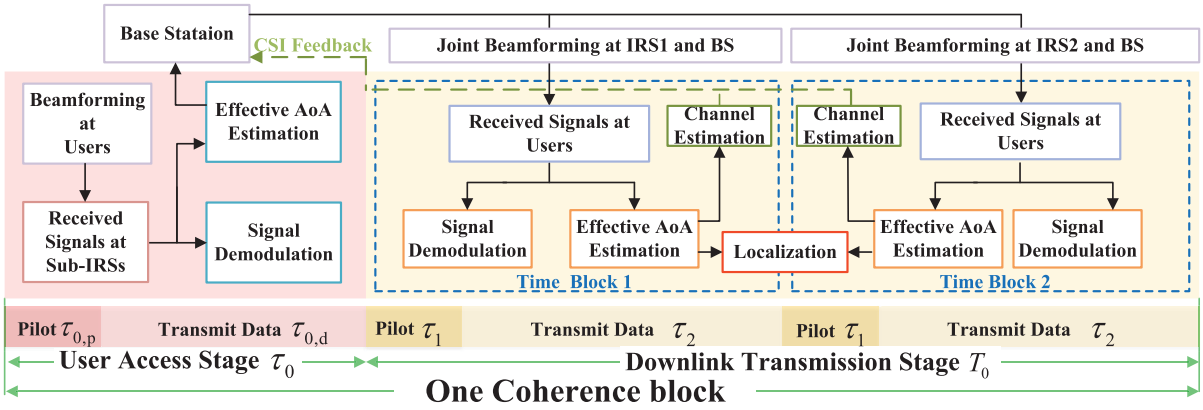

Fig. 2. A top-level diagram of the proposed I-CALL framework.

where $\mathbf{w}_{\mathrm{u},k} \in \mathbb{C}^{N_U \times 1}$, satisfying $\|\mathbf{w}_{\mathrm{u},k}\|^2 = 1$, is the transmit beamforming vector, which is random designed due to the unkown CSI. P_{u} denotes the transmit power at users. $\mathbf{H}_{\mathrm{U2I},j,k} \in \mathbb{C}^{M \times N_U}$ denotes the channel from the k-th user to the j-th sub-IRS, and $\mathbf{n}_{\mathrm{u}} \in \mathbb{C}^{M \times 1}$ is the additive white Gaussian noise (AWGN), whose elements follow the complex Gaussian distribution with zero mean and variance σ_{u}^2, i.e., $\mathcal{CN}\left(0, \sigma_{\mathrm{u}}^2\right)$.

2) Downlink Transmission Stage: Without loss of generality, we focus on the j-th time block of the second stage, during which the BS transmits symbols, i.e., $\mathbf{s}_{\mathrm{d},j,k} = [\mathbf{s}_{\mathrm{d},j,k}^{\mathrm{p}}, \mathbf{s}_{\mathrm{d},j,k}^{\mathrm{q}}]$, to the k-th user, where $\mathbf{s}_{\mathrm{d},j,k}^{\mathrm{p}} = [s_{\mathrm{d},j,k}(1), \cdots, s_{\mathrm{d},j,k}(\tau_1)]$ and $\mathbf{s}_{\mathrm{d},j,k}^{\mathrm{q}} = [s_{\mathrm{d},j,k}(\tau_1+1), \cdots, s_{\mathrm{d},j,k}(T_j)]$ denote the pilot symbols and the data symbols, respectively. $s_{d,j,k}(t)$ is the symbol transmitted at time slot $t \in \mathcal{T}_{\mathrm{d}} = \{1, \cdots, \tau_1, \cdots, T_j\}$. As we discussed in Section II-A, only one sub-IRS works during each time block, resulting in received signal as follows

$$\begin{aligned}&\mathbf{y}_{\mathrm{d},j,k}(t)\\ &= \mathbf{H}_{\mathrm{I2U},j,k}\mathbf{\Theta}_j\mathbf{H}_{\mathrm{B2I},j}\sum_{i=1}^{K}\mathbf{w}_{\mathrm{d},j,i}s_{\mathrm{d},j,i}(t) + \mathbf{n}_{\mathrm{d}}(t), j = 1, 2,\end{aligned} \tag{2}$$

where $\mathbf{H}_{\mathrm{I2U},j,k} \in \mathbb{C}^{N_U \times M}$ and $\mathbf{H}_{\mathrm{B2I},j} \in \mathbb{C}^{M \times N_B}$ denote the channels from the j-th sub-IRS to the k-th user and from the BS to the j-th sub-IRS, respectively. $\mathbf{w}_{\mathrm{d},j,i}$ is the beamforming vector with power constraint $\sum_{k=1}^{K}\|\mathbf{w}_{\mathrm{d},j,i}\|^2 \le P$, where P is the downlink transmit power at BS. The phase shift matrix of the j-th sub-IRS is defined as $\mathbf{\Theta}_j = \mathrm{diag}(\boldsymbol{\theta}_j)$, with the phase shift beam being $\boldsymbol{\theta}_j = \left[e^{\mathrm{j}\theta_{1,j}}, \cdots, e^{\mathrm{j}\theta_{M,j}}\right]^T \in \mathbb{C}^{M \times 1}$, where $\theta_{m,j} \in [0, 2\pi], \forall m = [1, \cdots, M]$ denotes the phase shift of the m-th element of the j-th sub-IRS. $\mathbf{n}_{\mathrm{d}}$ denotes the AWGN, whose elements follow the complex Gaussian distribution with $\mathcal{CN}\left(0, \sigma_{\mathrm{d}}^2\right)$.

C. Channel Model

We consider the IRS-assisted system working at mmWave frequency, where the channel from the BS to the j-th sub-IRS is modeled as in [26], [27], [28], [29]

$$\mathbf{H}_{\mathrm{B2I},j} = \sum_{l=1}^{L_{\mathrm{B2I},j}} \alpha_{\mathrm{B2I},j}^{l}\mathbf{a}_{\mathrm{I}}\left(u_{\mathrm{r,I},j}^{l}, v_{\mathrm{r,I},j}^{l}\right)\mathbf{a}_{\mathrm{B}}^{\mathrm{H}}\left(u_{\mathrm{t,B},j}^{l}\right), \tag{3}$$

where $L_{\mathrm{B2I},j}$ is the number of paths between the BS and the j-th sub-IRS and $\alpha_{\mathrm{B2I},j}^{l}$ represents the complex gain for the l-th path. The superscript "H" represents the Hermitian transpose. $\mathbf{a}_{\mathrm{B}}^{\mathrm{H}}\left(u_{\mathrm{t,B},j}^{l}\right)$ and $\mathbf{a}_{\mathrm{I}}\left(u_{\mathrm{r,I},j}^{l}, v_{\mathrm{r,I},j}^{l}\right)$ are the array response vector at the BS and the j-th sub-IRS, given as

$$\mathbf{a}_{\mathrm{B}}(u) = \left[1, \cdots, e^{j(n-1)u}, \cdots, e^{j(N_t-1)u}\right]^T. \tag{4}$$

$$\begin{aligned}\mathbf{a}(u,v) = &\left[1, \cdots, e^{j(n-1)u}, \cdots, e^{j(M_y-1)u}\right]^T\\ &\otimes \left[1, \cdots, e^{j(m-1)v}, \cdots, e^{j(M_z-1)v}\right]^T,\end{aligned} \tag{5}$$

The effective AoAs of the l-th path at the j-th sub-IRS $\{u_{\mathrm{r,I},j}^{l}, v_{\mathrm{r,I},j}^{l}\}$, and the effective angles of departure (AoDs) of the l-th path at the BS $u_{\mathrm{t,B},j}^{l}$, are defined as

$$\begin{aligned}u_{\mathrm{r,I},j}^{l} &= 2\pi\frac{d_{\mathrm{IRS}}}{\lambda}\cos\left(\gamma_{\mathrm{r,I},j}^{l}\right)\sin\left(\varphi_{\mathrm{r,I},j}^{l}\right),\\ v_{\mathrm{r,I},j}^{l} &= 2\pi\frac{d_{\mathrm{IRS}}}{\lambda}\sin\left(\gamma_{\mathrm{r,I},j}^{l}\right),\end{aligned} \tag{6}$$

$$u_{\mathrm{t,B,j}}^{l} = 2\pi\frac{d_{\mathrm{BS}}}{\lambda}\sin\left(\theta_{\mathrm{t,B},j}^{l}\right), \tag{7}$$

where λ denotes the carrier wavelength, d_{IRS} and d_{BS} represent the distances between two adjacent reflecting elements of the IRS and two adjacent antennas of the BS, respectively. $\gamma_{\mathrm{r,I},j}^{l}$ and $\varphi_{\mathrm{r,I},j}^{l}$ are the elevation and azimuth AoDs for the link from the BS to the j-th sub-IRS of the l-th path, and $\theta_{\mathrm{t,B},j}^{l}$ is the AoD of the l-th path at the BS.

The channel from the j-th sub-IRS to the k-th user is modeled as

$$\begin{aligned}&\mathbf{H}_{\mathrm{I2U},j,k}\\ &= \sum_{l=1}^{L_{\mathrm{I2U},j,k}} \alpha_{\mathrm{I2U},j,k}^{l}\mathbf{a}_{\mathrm{U}}\left(u_{\mathrm{r,U},j,k}^{l}, v_{\mathrm{r,U},j,k}^{l}\right)\mathbf{a}_{\mathrm{I}}^{\mathrm{H}}\left(u_{\mathrm{t,I},j,k}^{l}, v_{\mathrm{t,I},j,k}^{l}\right),\end{aligned} \tag{8}$$

where $L_{\mathrm{I2U},j,k}$ is the number of paths between the j-th sub-IRS and the k-th user. $\alpha_{\mathrm{I2U},j,k}^{l}$ represents the complex gain

for the l-th path. $\mathbf{a}_{\mathrm{U}}\left(u^l_{\mathrm{r,U},j,k}, v^l_{\mathrm{r,U},j,k}\right)$ is the array response vectors at the k-th user. The effective AoDs of the l-th path at the IRS, $\{u^l_{\mathrm{t,I},j,k}, v^l_{\mathrm{t,I},j,k}\}$, and the effective AoAs of the l-th path at the k-th user, $\{u^l_{\mathrm{r,U},j,k}, v^l_{\mathrm{r,U},j,k}\}$, are defined as

$$\begin{aligned} u^l_{\mathrm{t,I},j,k} &= 2\pi \frac{d_{\mathrm{IRS}}}{\lambda} \cos\left(\gamma^l_{\mathrm{t,I},j,k}\right) \sin\left(\varphi^l_{\mathrm{t,I},j,k}\right), \\ v^l_{\mathrm{t,I},j,k} &= 2\pi \frac{d_{\mathrm{IRS}}}{\lambda} \sin\left(\gamma^l_{\mathrm{t,U},j,k}\right), \end{aligned} \tag{9}$$

$$\begin{aligned} u^l_{\mathrm{r,U},j,k} &= 2\pi \frac{d_{\mathrm{USER}}}{\lambda} \cos\left(\gamma^l_{\mathrm{r,U},j,k}\right) \cos\left(\varphi^l_{\mathrm{r,U},j,k}\right), \\ v^l_{\mathrm{r,U},j,k} &= 2\pi \frac{d_{\mathrm{USER}}}{\lambda} \cos\left(\gamma^l_{\mathrm{r,U},j,k}\right) \sin\left(\varphi^l_{\mathrm{r,U},j,k}\right), \end{aligned} \tag{10}$$

where d_{USER} represent the distances between two adjacent antennas of the users, $\gamma^l_{\mathrm{t,I},j,k}$ and $\varphi^l_{\mathrm{t,I},j,k}$ are the elevation and azimuth AoDs for the link from the j-th sub-IRS to the k-th user of the l-th path, and $\gamma^l_{\mathrm{r,U},j,k}$ and $\varphi^l_{\mathrm{r,U},j,k}$ are the AoAs for the link from j-th IRS to the k-th user of the l-th path.

III. Design of User Access Stage

During the user access stage, the two sub-IRSs turn on the semi-passive elements and operate in the sensing mode. We first rewritten the received signals at the sub-IRSs in a more compact form. Define $\mathbf{A}^{\mathrm{u}}_{0,j} = \sqrt{P_{\mathrm{u}}}\left[\mathbf{H}_{\mathrm{U2I},j,1}\mathbf{w}_{\mathrm{u},1}, \cdots, \mathbf{H}_{\mathrm{U2I},j,K}\mathbf{w}_{\mathrm{u},K}\right] \in C^{M\times K}$, $\mathbf{Y}_{\mathrm{u},j} = [\mathbf{y}_{\mathrm{u},j}(1), \cdots, \mathbf{y}_{\mathrm{u},j}(\tau_0)] \in \mathbb{C}^{M\times\tau_0}$, $\mathbf{S}_{\mathrm{u}} = \left[\mathbf{s}^T_{\mathrm{u},1}, \cdots, \mathbf{s}^T_{\mathrm{u},K}\right]^T \in \mathbb{C}^{K\times\tau_0}$ and $\mathbf{N}_{\mathrm{u}} = [\mathbf{n}_{\mathrm{u}}(1), \cdots, \mathbf{n}_{\mathrm{u}}(\tau_0)] \in \mathbb{C}^{M\times\tau_0}$, the received signal can be written as follows

$$\mathbf{Y}_{\mathrm{u},j} = \mathbf{A}^{\mathrm{u}}_{0,j}\mathbf{S}_{\mathrm{u}} + \mathbf{N}_{\mathrm{u}} = \mathbf{X}_{0,j} + \mathbf{N}_{\mathrm{u}}, \tag{11}$$

which is a linear mixture with respect to the transmitted signal, and can be decomposed by utilizing the independent component analysis (ICA) technique [30]. In the following subsection, we estimate the symbols transmitted by the users and the effective AoAs at the j-th sub-IRS.

A. Uplink Symbol Detection

1) Signal Whitening: We first whiten the received signal through the principal component analysis (PCA) method to obtain the uncorrelated signal. The auto-correlation matrix, i.e., $\mathbf{R}_j \triangleq \mathbb{E}\left\{\mathbf{Y}_{\mathrm{u},j}\mathbf{Y}^H_{\mathrm{u},j}\right\}$ of the signal at the j-th sub-IRS can be estimated as

$$\hat{\mathbf{R}}_j = \frac{1}{\tau_0}\sum_{t=1}^{\tau_0}\mathbf{y}_{\mathrm{u},j}(t)\left[\mathbf{y}_{\mathrm{u},j}(t)\right]^H = \hat{\mathbf{R}}_{\mathrm{x},j} + \sigma^2_{\mathrm{u}}\mathbf{I} = \mathbf{U}_j\mathbf{\Lambda}_j\mathbf{U}^H_j, \tag{12}$$

where $\hat{\mathbf{R}}_{\mathrm{x},j}$ is the estimated auto-correlation matrix of $\mathbf{X}_{0,j}$ with rank K, $\mathbf{U}_j = [\mathbf{U}_{\mathrm{x},j}, \mathbf{U}_n]$ denotes the eigenvector and $\mathbf{\Lambda}_j = \begin{bmatrix} \mathbf{\Lambda}_{\mathbf{X},j} & \mathbf{0} \\ \mathbf{0} & \mathbf{\Lambda}_{\mathbf{N}} \end{bmatrix}$ denotes the eigenvalue. $\{\mathbf{U}_{\mathrm{x},j}, \mathbf{U}_n\}$, $\{\mathbf{\Lambda}_{\mathbf{X},j}, \mathbf{\Lambda}_{\mathbf{N}}\}$ are the eigenvector and eigenvalue matrix of signal $\mathbf{X}_{0,j}$ and noise $\mathbf{N}_{\mathrm{u}}$, respectively. The post-whiten signal $\mathbf{Y}_{\mathrm{u1},j} \in \mathbb{C}^{K\times\tau_0}$ is given by

$$\mathbf{Y}_{\mathrm{u1},j} = \mathbf{V}_j\mathbf{Y}_{\mathrm{u},j}, \tag{13}$$

where $\mathbf{V}_j = \mathbf{\Lambda}^{-1}_{\mathbf{X},j}\mathbf{U}_{\mathrm{x},j} \in \mathbb{C}^{K\times M}$ denotes the whitening matrix.

2) Phase Deviation and Permutation Correction: After obtaining $\mathbf{Y}_{\mathrm{u1},j}$, the joint approximative diagonalization of eigen-matrices (JADE) method is applied to exploit the high-order statistical properties of the whitened signal [31], [32]. Here we exploit the fourth-order statistical properties, i.e., the fourth-order cumulants of the whitened signal, $\mathfrak{C}\left(\mathbf{Y}_{\mathrm{u1},j}\right)$, to carry out the JADE process, which can be obtained by

$$\begin{aligned} \mathfrak{C}\left(\mathbf{Y}_{\mathrm{u1},j}\right) = &\frac{1}{\tau_0}\sum_{t=1}^{\tau_0}\left|\left[\mathbf{Y}_{\mathrm{u1},j}\right]_t\right|^4 - 2\left(\frac{1}{\tau_0}\sum_{t=1}^{\tau_0}\left|\left[\mathbf{Y}_{\mathrm{u1},j}\right]_t\right|^2\right)^2 \\ &- \frac{1}{\tau_0^2}\sum_{t=1}^{\tau_0}\sum_{l=1}^{\tau_0}\left(\left[\mathbf{Y}_{\mathrm{u1},j}\right]_t\right)^2\left(\left[\mathbf{Y}_{\mathrm{u1},j}\right]^*_l\right)^2. \end{aligned} \tag{14}$$

Then, we compute the K most significant eigenpairs, denoted by $\mathcal{N} = \{\lambda_k, \mathcal{M}_k \mid 1 \leqslant k \leqslant K\}$, where λ_k and $\mathcal{M}_k$ are the k-th largest eigenvalue and the corresponding eigenvector, respectively. Finally, we calculate the unitary matrix $\mathbf{G}$ by the Givens rotation method and jointly diagonalize the set $\mathcal{N}$. Therefore, the extracted signal and the linear mixing matrix are given by

$$\hat{\mathbf{S}}_{\mathrm{u1}} = \mathbf{G}^H\mathbf{Y}_{\mathrm{u1},j}, \ \hat{\mathbf{A}}^{\mathrm{u}}_{1,j} = \mathbf{Y}_{\mathrm{u},j}[\hat{\mathbf{S}}_{\mathrm{u1}}]^{\dagger}, \tag{15}$$

where the superscript "$\dagger$" represents the pseudo-inverse.

However, the ambiguity caused by the JADE method leads to the difference between the estimated signal and the transmitted signal, between the estimated linear mixing matrix and the original linear mixing matrix, which satisfy $\hat{\mathbf{S}}_{\mathrm{u1}} = \Delta\mathbf{S}_{\mathrm{u}}$, $\hat{\mathbf{A}}^{\mathrm{u}}_{1,j} = \mathbf{A}_{0,j}\Delta^{-1}$, where Δ is the ambiguity matrix. Fortunately, the ambiguity can be eliminated by a semi-blind receiver according to [33]. More specifically, the ambiguity can be decomposed into three parts, namely the phase deviation, the quadrant ambiguity, and the permutation ambiguity.

The first part, i.e., the phase deviation, is given by

$$\mathbf{P}^{-1} = diag\{p_1^{-1}, \cdots, p_K^{-1}\}, \tag{16}$$

where

$$p_k^{-1} = \frac{\left|\left(\frac{1}{\tau_0}\sum_{m=1}^{\tau_0}\left[\hat{\mathbf{S}}_{\mathbf{u}1}\right]^4_{k,m}\right)^{-\frac{1}{4}} e^{j\frac{\pi}{4}}\right|}{\left(\frac{1}{\tau_0}\sum_{m=1}^{\tau_0}\left[\hat{\mathbf{S}}_{\mathbf{u}1}\right]^4_{k,m}\right)^{-\frac{1}{4}} e^{j\frac{\pi}{4}}}. \tag{17}$$

The second part, i.e., the quadrant ambiguity, is given by

$$\mathbf{Q} = diag\{q_1, \cdots, q_K\}, \tag{18}$$

where $q_k = e^{-j\frac{\pi}{2}\arg\max_l\{\Re\left(\mathbf{r}^{\mathrm{p}}_k\right)\}}$. $\mathbf{r}^{\mathrm{p}}_k(l+1) = \frac{1}{\tau_{0,\mathrm{p}}}\sum_{m=1}^{\tau_{0,\mathrm{p}}}\left\{\left[\hat{\mathbf{S}}_{\mathrm{u1}}\right]_{k,m} e^{j\varphi_l}\left[\mathbf{s}^p_{u,k}\right]^*_m\right\}$ is the cross-correlation between the original and the extracted pilot symbols transmitted by the k-th user, $\varphi_l = \frac{\pi l}{2}, \forall l \in \{0,1,2,3\}$, and $\Re\left(\mathbf{r}^{\mathrm{p}}_k\right)$ stands for the real part of $\mathbf{r}^{\mathrm{p}}_k$.

The third part, i.e., the permutation deviation, is given by

$$[\mathbf{o}]_k = \arg\max_{l+1}|\mathbf{r}^{\mathrm{p}}_k|. \tag{19}$$

Algorithm 1 The BSE-SD Algorithm

1: **Input** the received signals $\mathbf{Y}_{\mathrm{u},j}$.
2: Whitening the received signals by (13).
3: Calculate the fourth-order cumulants $\mathfrak{C}(\mathbf{Y}_{\mathrm{u1},j})$ by (14).
4: Separate the signal $\hat{\mathbf{S}}_{\mathrm{u1}}$ and the mixing matrix $\hat{\mathbf{A}}^{\mathrm{u}}_{1,j}$ by (15).
5: Calculate the phase deviation matrix $\mathbf{P}$, the quadrant ambiguity $\mathbf{Q}$, and the permutation deviation $\mathbf{o}$ by (16), (18), and (19) respectively.
6: Estimate the transmitted signal $\hat{\mathbf{S}}_{\mathrm{u2}}$ and the mixing matrix $\hat{\mathbf{A}}^{\mathrm{u}}_{2,j}$ by (20).
7: **Output** the estimation of the transmit signals $\hat{\mathbf{S}}_{\mathrm{u2}}$ and the mixing matrix $\hat{\mathbf{A}}^{\mathrm{u}}_{2,j}$.

Thus, the estimated signal $\hat{\mathbf{S}}_{\mathrm{u2}}$ and the mixing matrix $\hat{\mathbf{A}}^{\mathrm{u}}_{2,j}$ is given by

$$\hat{\mathbf{S}}_{\mathrm{u2}} = \mathbf{Q}^{-1}\left[\mathbf{P}^{-1}\hat{\mathbf{S}}_{\mathrm{u1}}\right]_{(\mathbf{o},:)}, \hat{\mathbf{A}}^{\mathrm{u}}_{2,j} = \mathbf{Y}_{\mathrm{u},j}[\hat{\mathbf{S}}_{\mathrm{u2}}]^{\dagger}, \tag{20}$$

where the subscript $(\mathbf{o},:)$ implies that the rows of $\mathbf{P}^{-1}\hat{\mathbf{S}}_{\mathrm{u1}}$ are arranged in the order of elements in $\mathbf{o}$. For example, if $\mathbf{o} = [3,1,2]^H$ and $\mathbf{B} = [\mathbf{b}_1^T, \mathbf{b}_2^T, \mathbf{b}_3^T]$, then $[\mathbf{B}]_{(\mathbf{o},:)} = [\mathbf{b}_3^T, \mathbf{b}_1^T, \mathbf{b}_2^T]$.

The algorithm for blind source estimation and the signal demodulation (BSE-SD) is summarized in **Algorithm 1**.

B. Effective AoA Estimation

In this subsection, the effective AoAs from the k-th user to the j-th sub-IRS corresponding to the y axis and the z axis are separately estimated by using total least square (TLS) estimation of signal parameters via rotational invariance technique (ESPRIT) method based on the estimated mixing matrix (i.e., $\hat{\mathbf{A}}^{\mathrm{u}}_{2,j}$). Then, the effective AoAs are paired by the multiple signal classification (MUSIC) method.

It is observed that the k-th column of the mixing matrix $\mathbf{A}^{\mathrm{u}}_{0,j}$ corresponds to the product of the channel and the beamforming vector from the k-th user to the j-th sub-IRS, i.e., $\mathbf{A}^{\mathrm{u}}_{0,j} = \sqrt{P_{\mathrm{u}}}[\mathbf{H}_{\mathrm{U2I},j,1}\mathbf{w}_{\mathrm{u},1}, \cdots, \mathbf{H}_{\mathrm{U2I},j,K}\mathbf{w}_{\mathrm{u},K}]$. Recall (1) and let $\left[\mathbf{A}^{\mathrm{u}}_{0,j}\right]_{(:,k)}$ denote the k-th column of $\mathbf{A}^{\mathrm{u}}_{0,j}$, which satisfies

$$\begin{aligned}&\left[\mathbf{A}^{\mathrm{u}}_{0,j}\right]_{(:,k)}\\ &= \sum_{l=1}^{L_{\mathrm{I2U},j,k}} \alpha^{l}_{\mathrm{I2U},j,k}\mathbf{a}_{\mathrm{I}}\left(u^{l}_{\mathrm{r,I},j,k}, v^{l}_{\mathrm{r,I},j,k}\right)\mathbf{a}^{\mathrm{H}}_{\mathrm{U}}\left(u^{l}_{\mathrm{t,U},j,k}, v^{l}_{\mathrm{t,U},j,k}\right)\mathbf{w}_{\mathrm{u},k}\\ &= \mathbf{B}^{\mathrm{u}}_{\mathrm{I},j,k}\mathbf{e}^{\mathrm{u}}_{\mathrm{U},j,k},\end{aligned} \tag{21}$$

where $\{u^{l}_{\mathrm{r,I},j,k}, v^{l}_{\mathrm{r,I},j,k}\}$ and $\{u^{l}_{\mathrm{t,U},j,k}, v^{l}_{\mathrm{t,U},j,k}\}$ represent the effective AoAs at the j-th sub-IRS, and the effective AoD at the k-th user in user access stage, respectively,

$$\mathbf{B}^{\mathrm{u}}_{\mathrm{I},j,k} = \left[\mathbf{a}_{\mathrm{I}}\left(u^{1}_{\mathrm{r,I},j,k}, v^{1}_{\mathrm{r,I},j,k}\right), \cdots, \mathbf{a}_{\mathrm{I}}\left(u^{L_{\mathrm{I2U},j,k}}_{\mathrm{r,I},j,k}, v^{L_{\mathrm{I2U},j,k}}_{\mathrm{r,I},j,k}\right)\right], \tag{22}$$

and

$$\mathbf{e}^{\mathrm{u}}_{\mathrm{U},j,k} = [\alpha^{1}_{\mathrm{I2U},j,k}\mathbf{a}^{\mathrm{H}}_{\mathrm{U}}\left(u^{1}_{\mathrm{t,U},j,1}, v^{1}_{\mathrm{t,U},j,1}\right)\mathbf{w}_{\mathrm{u},k}, \cdots, \alpha^{L_{\mathrm{I2U},j,k}}_{\mathrm{I2U},j,k}\mathbf{a}^{\mathrm{H}}_{\mathrm{U}}\left(u^{L_{\mathrm{I2U},j,k}}_{\mathrm{t,U},j,K}, v^{L_{\mathrm{I2U},j,k}}_{\mathrm{t,U},j,k}\right)\mathbf{w}_{\mathrm{u},k}]^T. \tag{23}$$

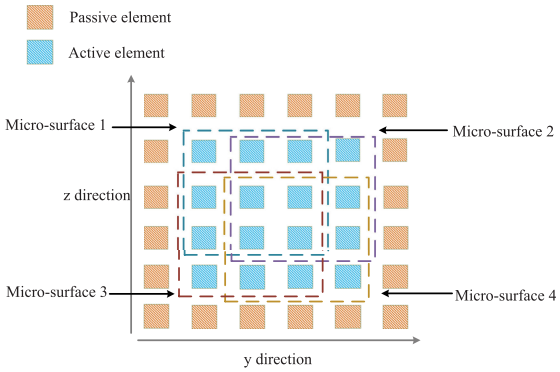

Fig. 3. The example of the micro-surfaces.

Then, the effective AoAs can be estimated by applying the TLS ESPRIT method, independently.

Before applying the TLS ESPRIT method to estimate the effective AoAs, the forward-backward spatial smoothing (FBSS) [34] method is used to preprocess the estimated mixing matrix. Specifically, all the semi-passive reflecting elements of the j-th sub-IRS constitute a set of $N_{\mathrm{m},j}$ micro-surfaces each with $L_{\mathrm{m},j} = Q_{y,j} \times Q_{z,j}$ elements. Fig. 3 shows an example of the micro-surfaces, where a set of 4 micro-surfaces, each with 3×3 semi-passive elements, are constructed.[6] With the processing of FBSS technology, the auto-correlation matrix at the m-th micro-surface, i.e., $\mathbf{R}^{\mathrm{u}}_{1,j,k} \triangleq \mathbb{E}\left\{\left[\hat{\mathbf{A}}^{\mathrm{u}}_{2,j}\right]_{(:,k),m}\left(\left[\hat{\mathbf{A}}^{\mathrm{u}}_{2,j}\right]_{(:,k),m}\right)^H\right\}$, can be estimated as

$$\begin{aligned}\hat{\mathbf{R}}^{\mathrm{u}}_{1,j,k} &= \frac{1}{2N_{\mathrm{m},j}}\sum_{m=1}^{N_{\mathrm{m},j}}\left\{\left[\hat{\mathbf{A}}^{\mathrm{u}}_{2,j}\right]_{(:,k),m}\left(\left[\hat{\mathbf{A}}^{\mathrm{u}}_{2,j}\right]_{(:,k),m}\right)^H\right.\\ &\quad\left.+\mathbf{J}\left(\left[\hat{\mathbf{A}}^{\mathrm{u}}_{2,j}\right]_{(:,k),m}\right)^*\left(\left[\hat{\mathbf{A}}^{\mathrm{u}}_{2,j}\right]_{(:,k),m}\right)^T\mathbf{J}\right\}\\ &= \mathbf{U}^{(1)}_{j,k}\,\mathrm{diag}\left(\lambda^{(1)}_{j,,k1}, \ldots, \lambda^{(1)}_{j,k,L_{\mathrm{m},j}}\right)\left[\mathbf{U}^{(1)}_{j,k}\right]^H,\end{aligned} \tag{24}$$

where $\mathbf{J}$ is the exchange matrix with element 1 only residing on its counter-diagonal and all other elements being zero, $\mathbf{U}^{(1)}_{j,k} = [\mathbf{u}^{(1)}_{j,k,1}, \cdots, \mathbf{u}^{(1)}_{j,k,L_{\mathrm{m},j}}]$, and the eigenvalues $\lambda^{(1)}_{j,1}, \cdots, \lambda^{(1)}_{j,k,L_{\mathrm{m},j}}$ are in descending order.

The process of estimating the effective AoAs is as follows:

1) Estimate $u^{l}_{\mathrm{r,I},j,k}$ by Using the TLS ESPRIT Algorithm: For the j-th sub-IRS, we first construct two auxiliary sub-surfaces as illustrated in Fig. 4(a), each with the size of $L^{(1)}_{\mathrm{aux},j} = (Q_{y,j} - 1) \times Q_{z,j}$. The signal sub-space is

$$\mathbf{U}^{(1)}_{\mathrm{S},j,k,z} \triangleq \mathbf{J}_z\mathbf{U}^{(1)}_{\mathrm{S},j,k}, z = 1, 2, \tag{25}$$

where $\mathbf{U}^{(1)}_{\mathrm{S},j,k} \triangleq \left[\mathbf{u}^{(1)}_{j,k,1}, \cdots, \mathbf{u}^{(1)}_{j,k,L_{\mathrm{I2U},j,k}}\right] \in \mathbb{C}^{L_{\mathrm{m},i} \times L_{\mathrm{I2U},j,k}}$ and $\mathbf{J}_z \in \mathbb{R}^{L_{\mathrm{aux},i} \times L_{\mathrm{m,i}}}$ is a selecting matrix. $[\mathbf{J}_z]_{nm} = 1$ if the m-th reflecting element of the micro-surface 1 is selected

[6] Therefore, the impact of M_a is reflected in $L_{\mathrm{m},j}$, $Q_{y,j}$, and $Q_{z,j}$, from Eq. (24) to Eq. (30).

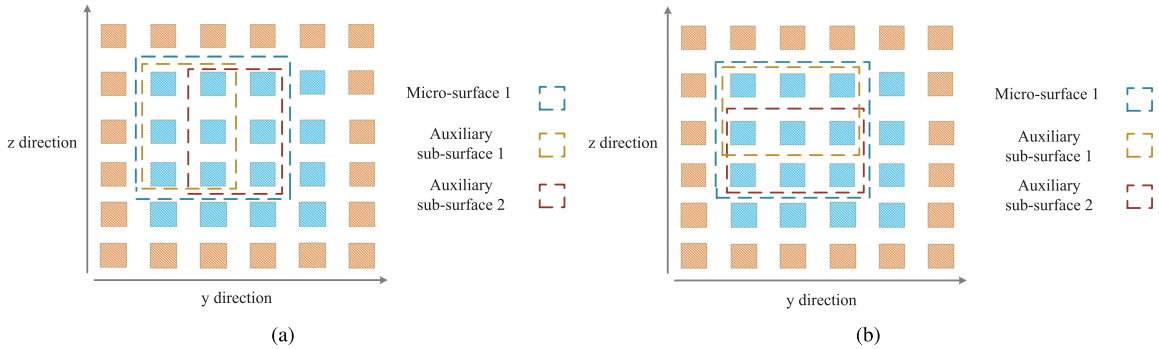

Fig. 4. The example of the auxiliary sub-surfaces.

as the n-th element of the auxiliary sub-surface, and otherwise $[\mathbf{J}_z]_{nm} = 0$.

Then, we define $\mathbf{C}^{(1)}_{j,k} \triangleq \left[\mathbf{U}^{(1)}_{\mathrm{S},j,k,1}, \mathbf{U}^{(1)}_{\mathrm{S},j,k,2}\right]^H \left[\mathbf{U}^{(1)}_{\mathrm{S},j,k,1}, \mathbf{U}^{(1)}_{\mathrm{S},j,k,2}\right]$, and perform eigen-decomposition, which yields

$$\mathbf{C}^{(1)}_{j,k} = \begin{bmatrix} \mathbf{V}^{(1)}_{j,k,11} & \mathbf{V}^{(1)}_{j,k,12} \\ \mathbf{V}^{(1)}_{j,k,21} & \mathbf{V}^{(1)}_{j,k,22} \end{bmatrix} \mathbf{\Lambda}^{(1)}_{\mathrm{C},j,k} \begin{bmatrix} \mathbf{V}^{(1)}_{j,k,11} & \mathbf{V}^{(1)}_{j,k,12} \\ \mathbf{V}^{(1)}_{j,k,21} & \mathbf{V}^{(1)}_{j,k,22} \end{bmatrix}^H, \tag{26}$$

where $\mathbf{\Lambda}^{(1)}_{\mathrm{C},j,k} \triangleq \mathrm{diag}\left(\lambda^{(1)}_{\mathrm{C},j,k,1}, \ldots, \lambda^{(1)}_{\mathrm{C},j,k,2L_{\mathrm{U2I},j,k}}\right)$ with the eigenvalues in a decreasing order, and $\mathbf{V}^{(1)}_{j,k,12}$ and $\mathbf{V}^{(1)}_{j,k,22}$ are the eigenmatrix of size $L_{\mathrm{I2U},j,k} \times L_{\mathrm{I2U},j,k}$.

After obtaining $\mathbf{V}^{(1)}_{j,k,12}$ and $\mathbf{V}^{(1)}_{j,k,22}$, we can calculate

$$\Phi^{(1)}_{\mathrm{TLS},j,k} = -\mathbf{V}^{(1)}_{j,k,12} \left[\mathbf{V}^{(1)}_{j,k,22}\right]^{-1}. \tag{27}$$

By performing eigen-decomposition of $\Phi^{(1)}_{\mathrm{TLS},j,k}$, its eigenvalues $\lambda^{(1)}_{\mathrm{TLS},j,k,l}$ can be obtained. Then, we get the effective AoAs at the j-th sub-IRS corresponding to the y axis, which can be estimated as

$$\hat{u}^l_{\mathrm{r,I},j,k} = \mathrm{angle}\left(\lambda^{(1)}_{\mathrm{TLS},j,k,l}\right), l = 1, \cdots, L_{\mathrm{I2U},j,k}. \tag{28}$$

2) Estimate $v^l_{\mathrm{r,I},j,k}$ by Using the TLS ESPRIT Algorithm: For the j-th sub-IRS, two auxiliary sub-surfaces, with the size of $L^{(2)}_{\mathrm{aux},j} = (Q_{y,j}) \times Q_{z,j} - 1$, are constructed as illustrated in Fig. 4(b). Similar to the process of estimating $\hat{u}^l_{\mathrm{r,I},j,k}$, the effective AoAs can be estimated as $\hat{v}^l_{\mathrm{r,I},j,k}$.

3) Pair All the Effective AoAs, i.e., $\hat{u}^l_{\mathrm{r,I},j,k}$ and $\hat{v}^l_{\mathrm{r,I},j,k}$, by Using MUSIC Algorithm: Let

$$\check{f}^{(l,s)}_{j,k} \triangleq \mathbf{b}^H_{\mathrm{m},j}\left(\hat{u}^l_{\mathrm{r,I},j,k}, \hat{u}^s_{\mathrm{r,I},j,k}\right) \mathbf{U}^{(1)}_{\mathrm{N},j,k}, \tag{29}$$

where $\mathbf{U}^{(1)}_{\mathbf{N}_\mathrm{u},j,k} \triangleq \left[\mathbf{u}^{(1)}_{j,k,L_{\mathrm{I2U},j,k}+1}, \ldots, \mathbf{u}^{(1)}_{j,k,L_{\mathrm{m},j}}\right] \in \mathbb{C}^{L_{\mathrm{m},j} \times (L_{\mathrm{m},j} - L_{\mathrm{I2U},j,k})}$, and $\mathbf{b}_{\mathrm{m},j}$ is the array response vector of the micro-surfaces on the j-th sub-IRS. Then we compute

$$f\left(\hat{u}^l_{\mathrm{r,I},j,k}, \hat{u}^l_{\mathrm{r,I},j,k}\right) = \check{f}^{(l,s)}_{j,k}\left[\check{f}^{(l,s)}_{j,k}\right]^H, l, s = 1, \cdots, L_{\mathrm{I2U},j,k}, \tag{30}$$

and choose the $L_{\mathrm{I2U},j,k}$ minima $f\left(\hat{u}^l_{\mathrm{r,I},j,k}, \hat{u}^l_{\mathrm{r,I},j,k}\right)$ to obtain the effective AoA pairs $\left(\hat{u}^l_{\mathrm{r,I},j,k}, \hat{v}^l_{\mathrm{r,I},j,k}\right)$.

Algorithm 2 The E-Angle Algorithm

1: **for** $k = 1$ to K **do**
2: **Input** the estimated linear mixing vector $\left[\hat{\mathbf{A}}^{\mathrm{u}}_{2,j}\right]_{(k,:)}$.
3: Smoothing $\left[\hat{\mathbf{A}}^{\mathrm{u}}_{2,j}\right]_{(k,:),m}$ by the FBSS method by (24).
4: Using the TLS ESPRIT algorithm from (25) to (28) to estimate $u^l_{\mathrm{r,I},j,k}$ corresponding to the y axis and $v^l_{\mathrm{r,I},j,k}$ corresponding to the z axis.
5: Pair all the effective AoAs, i.e., $\hat{u}^l_{\mathrm{r,I},j,k}$ and $\hat{v}^l_{\mathrm{r,I},j,k}$, by (30).
6: **end for**
7: **Output** the estimation of the effective AoAs $\{\hat{u}^l_{\mathrm{r,I},j,k}, \hat{v}^l_{\mathrm{r,I},j,k}\}$.

Remark 1: In the TLS ESPRIT method, the eigenvalues and the corresponding eigenvectors are arranged in descending order, thus, the l-th estimated effective AoA pair $\{\hat{u}^l_{\mathrm{r,I},j,k}, \hat{v}^l_{\mathrm{r,I},j,k}\}$ may not correspond to the effective AoA pairs $\{u^l_{\mathrm{r,I},j,k}, v^l_{\mathrm{r,I},j,k}\}$ from the k-th user to the j-th sub-IRS via l-th path, which results in the AoA pairs mismatch. However, this mismatch can be solved by the proposed two-stage algorithm proposed in Section IV.

The algorithm for the effective AoAs estimation (E-angle) is summarized in **Algorithm 2**.

Up to this point, we have focused on the processing involved in the user access stage, which encompasses the BSE-SD algorithm for detecting the transmit signal and the E-angle algorithm for estimating effective AoAs. The subsequent section will delve into the processing techniques used during downlink transmission stage.

IV. Design of Downlink Transmission Stage

In this section, we first introduce the proposed beamforming scheme. Then, the downlink symbol demodulation, angle estimation, channel estimation, and localization approaches will be elaborated, followed by the overall complexity analysis.

Without loss of generality, we focus on the j-th time block. Inspired by radar communication systems, which improves the signal quality by maximizing a desired transmit beampattern or minimizing the cross-correlation between the transmit signals at various directions without relying on prior knowledge about the target [35], [36], [37], we propose a beamforming design

scheme that utilizes the effective AoAs estimated at the sub-IRSs during the first stage.

A. Beamforming Design

Since the LoS and NLoS paths between the sub-IRSs and the user cannot be distinguished, it is important to take beampattern among all the effective AoAs into consideration for fairness. Inspired by the works [35], [36], [37], we aim at minimizing the maximum weighted auto-correlation and cross-correlation beampattern gain among all the users, and the optimization problem is formulated as

$$\text{(P1)}: \min_{\boldsymbol{\Theta}_j, \mathbf{w}_{\mathrm{d},j,k}} \max_k -\varrho f_{1,j,k}+f_{2,j,k}+f_{3,j,k}+f_{4,j,k}, \tag{31a}$$

$$\text{s.t.} \quad \sum_{k=1}^{K} \|\mathbf{w}_{\mathrm{d},j,k}\|^2 \le P, \tag{31b}$$

$$|\boldsymbol{\Theta}_j| = \mathbf{I}, \tag{31c}$$

where ϱ denotes the weighting factor and

$$f_{1,j,k} = \sum_{L_{\mathrm{I2U},j,k}}^{L} \left|\mathbf{a}_{\mathrm{I}}^{\mathrm{H}}\left(\hat{u}_{\mathrm{t,I},j,k}^{l}, \hat{v}_{\mathrm{t,I},j,k}^{l}\right) \boldsymbol{\Theta}_j \mathbf{H}_{\mathrm{B2I},j} \mathbf{w}_{d,j,k}\right|^2, \tag{32}$$

represents the desired transmit beampattern gain for the k-th user at directions $\{\hat{u}_{\mathrm{t,I},j,k}^{l}, \hat{v}_{\mathrm{t,I},j,k}^{l}\}$.

$$f_{2,j,k} = \frac{2}{{L_{\mathrm{I2U},j,k}}^2 - L_{\mathrm{I2U},j,k}} \sum_{l=1}^{L_{\mathrm{I2U},j,k}-1} \sum_{p=l+1}^{L_{\mathrm{I2U},j,k}} \left|\mathbf{a}_I^H\left(\hat{u}_{\mathrm{t,I},j,k}^{l}, \hat{v}_{\mathrm{t,I},j,k}^{l}\right) \boldsymbol{\Theta}_j \mathbf{H}_{\mathrm{B2I},j} \mathbf{w}_{\mathrm{d},j,k} \mathbf{w}_{\mathrm{d},j,k}^H \mathbf{H}_{\mathrm{B2I},j}^H \boldsymbol{\Theta}_j^H \mathbf{a}_I\left(\hat{u}_{\mathrm{t,I},j,k}^{p}, \hat{v}_{\mathrm{t,I},j,k}^{p}\right)\right|^2, \tag{33}$$

denotes the cross-correlation for the k-th user between the directions $\{\hat{u}_{\mathrm{t,I},j,k}^{p}, \hat{v}_{\mathrm{t,I},j,k}^{p}\}$ and $\{\hat{u}_{\mathrm{t,I},j,k}^{l}, \hat{v}_{\mathrm{t,I},j,k}^{l}\}$.

$$f_{3,j,k} = \frac{2}{{L_{\mathrm{I2U},j,k}}^2 - L_{\mathrm{I2U},j,k}} \sum_{l=1}^{L_{\mathrm{I2U},j,k}-1} \sum_{p=l+1}^{L_{\mathrm{I2U},j,k}} \left|\mathbf{a}_I^H\left(\hat{u}_{\mathrm{t,I},j,k}^{l}, \hat{v}_{\mathrm{t,I},j,k}^{l}\right) \boldsymbol{\Theta}_j \mathbf{H}_{\mathrm{B2I},j} \sum_{i\neq k}^{K} \mathbf{w}_{\mathrm{d},j,i} \mathbf{w}_{\mathrm{d},j,i}^H \mathbf{H}_{\mathrm{B2I},j}^H \boldsymbol{\Theta}_j^H \mathbf{a}_I\left(\hat{u}_{\mathrm{t,I},j,k}^{p}, \hat{v}_{\mathrm{t,I},j,k}^{p}\right)\right|^2, \tag{34}$$

signifies the cross-correlation, corresponding to the inter-user-interference, between the directions $\{\hat{u}_{\mathrm{t,I},j,k}^{p}, \hat{v}_{\mathrm{t,I},j,k}^{p}\}$ and $\{\hat{u}_{\mathrm{t,I},j,k}^{l}, \hat{v}_{\mathrm{t,I},j,k}^{l}\}$, and

$$f_{4,j,k} = \frac{1}{L_{\mathrm{I2U},j,k}} \sum_{L_{\mathrm{I2U},j,k}}^{L} \left|\mathbf{a}_{\mathrm{I}}^{\mathrm{H}}\left(\hat{u}_{\mathrm{t,I},j,k}^{l}, \hat{v}_{\mathrm{t,I},j,k}^{l}\right) \boldsymbol{\Theta}_j \mathbf{H}_{\mathrm{B2I},j} \sum_{i\neq k}^{K} \mathbf{w}_{d,j,i} \mathbf{w}_{d,j,i}^H \mathbf{H}_{\mathrm{B2I},j}^H \boldsymbol{\Theta}_j^H \mathbf{a}_{\mathrm{I}}\left(\hat{u}_{\mathrm{t,I},j,k}^{l}, \hat{v}_{\mathrm{t,I},j,k}^{l}\right)\right|^2, \tag{35}$$

denotes the beampattern gain, corresponding to the inter-user-interference at directions $\{\hat{u}_{\mathrm{t,I},j,k}^{l}, \hat{v}_{\mathrm{t,I},j,k}^{l}\}$, where the effective AoDs, $\hat{u}_{\mathrm{t,I},j,k}^{l}$ and $\hat{v}_{\mathrm{t,I},j,k}^{l}$, are obtained in the first stage due to the reciprocity of the channels, i.e. $\mathbf{H}_{\mathrm{U2I},j,k} = \mathbf{H}_{\mathrm{I2U},j,k}^{T}$. It should be noted that for the k-th user, the weighted auto-correlation and cross-correlation beampattern gain, i.e., $-\varrho f_{1,j,k}$ and $f_{2,j,k}$, as well as the inter-user interference from the i-th ($i \neq k$) user i.e., $f_{3,j,k}$ and $f_{4,j,k}$, should be minimized to reduce the interference.

The above optimization problem is highly nonconvex with coupled variables, hence the optimal solution is difficult to obtain. However, by using alternating optimization methods [7], the active beamforming at the BS and the passive beamforming at the j-th sub-IRS can be properly optimized as follows:

1) Optimize $\mathbf{w}_{\mathrm{d},j,k}$ With Given $\boldsymbol{\Theta}_j$: With given $\boldsymbol{\Theta}_j$, the above problem can be rewritten as

$$\text{(P2-1)}: \min_{\mathbf{W}_{\mathrm{d},j,k}} \max_k -\varrho f_{1,j,k}^{\mathrm{w}}+f_{2,j,k}^{\mathrm{w}}+f_{3,j,k}^{\mathrm{w}}+f_{4,j,k}^{\mathrm{w}}, \tag{36a}$$

$$\text{s.t.} \quad \mathrm{rank}(\mathbf{W}_{\mathrm{d},j,k}) = 1, \tag{36b}$$

$$(31b), \tag{36c}$$

where $\mathbf{W}_{\mathrm{d},j,k} = \mathbf{w}_{\mathrm{d},j,k}\mathbf{w}_{\mathrm{d},j,k}^H$, and

$$f_{1,j,k}^{\mathrm{w}} = \sum_{L_{\mathrm{I2U},j,k}}^{L} \mathbf{a}_{\mathrm{I}}^{\mathrm{H}}\left(\hat{u}_{\mathrm{t,I},j,k}^{l}, \hat{v}_{\mathrm{t,I},j,k}^{l}\right) \boldsymbol{\Theta}_j \mathbf{H}_{\mathrm{B2I},j} \mathbf{W}_{d,j,k} \mathbf{H}_{\mathrm{B2I},j} \boldsymbol{\Theta}_j \mathbf{a}_{\mathrm{I}}\left(\hat{u}_{\mathrm{t,I},j,k}^{l}, \hat{v}_{\mathrm{t,I},j,k}^{l}\right), \tag{37}$$

$$f_{2,j,k}^{\mathrm{w}} = \frac{2}{{L_{\mathrm{I2U},j,k}}^2 - L_{\mathrm{I2U},j,k}} \sum_{l=1}^{L_{\mathrm{I2U},j,k}-1} \sum_{p=l+1}^{L_{\mathrm{I2U},j,k}} \left|\mathbf{a}_I^H\left(\hat{u}_{\mathrm{t,I},j,k}^{l}, \hat{v}_{\mathrm{t,I},j,k}^{l}\right) \boldsymbol{\Theta}_j \mathbf{H}_{\mathrm{B2I},j} \mathbf{W}_{\mathrm{d},j,k} \mathbf{H}_{\mathrm{B2I},j}^H \boldsymbol{\Theta}_j^H \mathbf{a}_I\left(\hat{u}_{\mathrm{t,I},j,k}^{p}, \hat{v}_{\mathrm{t,I},j,k}^{p}\right)\right|^2, \tag{38}$$

$$f_{3,j,k}^{\mathrm{w}} = \frac{2}{{L_{\mathrm{I2U},j,k}}^2 - L_{\mathrm{I2U},j,k}} \sum_{l=1}^{L_{\mathrm{I2U},j,k}-1} \sum_{p=l+1}^{L_{\mathrm{I2U},j,k}} \left|\mathbf{a}_I^H\left(\hat{u}_{\mathrm{t,I},j,k}^{l}, \hat{v}_{\mathrm{t,I},j,k}^{l}\right) \boldsymbol{\Theta}_j \mathbf{H}_{\mathrm{B2I},j} \sum_{i\neq k}^{K} \mathbf{W}_{\mathrm{d},j,i} \mathbf{H}_{\mathrm{B2I},j}^H \boldsymbol{\Theta}_j^H \mathbf{a}_I\left(\hat{u}_{\mathrm{t,I},j,k}^{p}, \hat{v}_{\mathrm{t,I},j,k}^{p}\right)\right|^2, \tag{39}$$

and

$$f_{4,j,k}^{\mathrm{w}} = \frac{1}{L_{\mathrm{I2U},j,k}} \sum_{L_{\mathrm{I2U},j,k}}^{L} \left|\mathbf{a}_{\mathrm{I}}^{\mathrm{H}}\left(\hat{u}_{\mathrm{t,I},j,k}^{l}, \hat{v}_{\mathrm{t,I},j,k}^{l}\right) \boldsymbol{\Theta}_j \mathbf{H}_{\mathrm{B2I},j} \sum_{i\neq k}^{K} \mathbf{W}_{d,j,i} \mathbf{H}_{\mathrm{B2I},j}^H \boldsymbol{\Theta}_j^H \mathbf{a}_{\mathrm{I}}\left(\hat{u}_{\mathrm{t,I},j,k}^{l}, \hat{v}_{\mathrm{t,I},j,k}^{l}\right)\right|^2. \tag{40}$$

The optimization problem (P2-1) is still non-convex because of the rank-one constraints. Omitting these constraints leads to the following relaxation[7]:

$$\text{(P2-2)}: \min_{\mathbf{W}_{\mathrm{d},j,k}} \max_k -\varrho f_{1,j,k}^{\mathrm{w}}+f_{2,j,k}^{\mathrm{w}}+f_{3,j,k}^{\mathrm{w}}+f_{4,j,k}^{\mathrm{w}}, \tag{41a}$$

$$\text{s.t.} \quad (31b), \tag{41b}$$

The above problem can be efficiently solved in polynomial time using the semi-definite quadratic programming (SQP) techinque as in [37], [38], and [39].

[7]Note that the rank-1 constraint can be satisfied by eigen-decomposition method or Gaussian Randomization method [46].

2) Optimize $\mathbf{\Theta}_j$ With Given $\mathbf{w}_{\mathrm{d},j,k}$: Similarly, with given $\mathbf{w}_{\mathrm{d},j,k}$, the above problem can be rewritten as

$$\text{(P3-1)}: \min_{\mathbf{V}_j} \max_k \; -\varrho f^{\mathrm{v}}_{1,j,k} + f^{\mathrm{v}}_{2,j,k} + f^{\mathrm{v}}_{3,j,k} + f^{\mathrm{v}}_{4,j,k}, \tag{42a}$$

$$\text{s.t.} \quad \mathrm{rank}(\mathbf{V}_j) = 1, \tag{42b}$$

$$(31c), \tag{42c}$$

where $\mathbf{V}_j = \mathbf{\Theta}_j \mathbf{\Theta}_j^H$, and

$$f^{\mathrm{v}}_{1,j,k} = \sum_{L_{\mathrm{I2U},j,k}}^{L} \mathbf{w}^T_{d,j,k} \mathbf{H}^T_{\mathrm{B2I},j} \mathrm{diag}\left(\mathbf{a}^*_{\mathrm{I}}\left(\hat{u}^l_{\mathrm{t,I},j,k}, \hat{v}^l_{\mathrm{t,I},j,k}\right)\right) \mathbf{V}_j \mathrm{diag}\left(\mathbf{a}^{\mathrm{T}}_{\mathrm{I}}\left(\hat{u}^l_{\mathrm{t,I},j,k}, \hat{v}^l_{\mathrm{t,I},j,k}\right)\right) \mathbf{H}^*_{\mathrm{B2I},j} \mathbf{w}^*_{d,j,k}, \tag{43}$$

$$f^{\mathrm{v}}_{2,j,k} = \frac{2}{{L_{\mathrm{I2U},j,k}}^2 - L_{\mathrm{I2U},j,k}} \sum_{l=1}^{L_{\mathrm{I2U},j,k}-1} \sum_{p=l+1}^{L_{\mathrm{I2U},j,k}} \left| \mathbf{w}^T_{d,j,k} \mathbf{H}^T_{\mathrm{B2I},j} \mathrm{diag}\left(\mathbf{a}^*_{\mathrm{I}}\left(\hat{u}^p_{\mathrm{t,I},j,k}, \hat{v}^p_{\mathrm{t,I},j,k}\right)\right) \mathbf{V}_j \mathrm{diag}\left(\mathbf{a}^{\mathrm{T}}_{\mathrm{I}}\left(\hat{u}^l_{\mathrm{t,I},j,k}, \hat{v}^l_{\mathrm{t,I},j,k}\right)\right) \mathbf{H}^*_{\mathrm{B2I},j} \mathbf{w}^*_{d,j,k} \right|^2, \tag{44}$$

$$f^{\mathrm{v}}_{3,j,k} = \frac{2}{{L_{\mathrm{I2U},j,k}}^2 - L_{\mathrm{I2U},j,k}} \sum_{l=1}^{L_{\mathrm{I2U},j,k}-1} \sum_{p=l+1}^{L_{\mathrm{I2U},j,k}} \left| \sum_{i\neq k}^{K} \mathbf{w}^T_{d,j,i} \mathbf{H}^T_{\mathrm{B2I},j} \mathrm{diag}\left(\mathbf{a}^*_{\mathrm{I}}\left(\hat{u}^p_{\mathrm{t,I},j,k}, \hat{v}^p_{\mathrm{t,I},j,k}\right)\right) \mathbf{V}_j \mathrm{diag}\left(\mathbf{a}^{\mathrm{T}}_{\mathrm{I}}\left(\hat{u}^l_{\mathrm{t,I},j,k}, \hat{v}^l_{\mathrm{t,I},j,k}\right)\right) \mathbf{H}^*_{\mathrm{B2I},j} \mathbf{w}^*_{d,j,i} \right|^2, \tag{45}$$

and

$$f^{\mathrm{v}}_{4,j,k} = \frac{1}{L_{\mathrm{I2U},j,k}} \sum_{L_{\mathrm{I2U},j,k}}^{L} \left| \sum_{i\neq k}^{K} \mathbf{w}^T_{d,j,i} \mathbf{H}^T_{\mathrm{B2I},j} \mathrm{diag}\left(\mathbf{a}^*_{\mathrm{I}}\left(\hat{u}^l_{\mathrm{t,I},j,k}, \hat{v}^l_{\mathrm{t,I},j,k}\right)\right) \mathbf{V}_j \mathrm{diag}\left(\mathbf{a}^{\mathrm{T}}_{\mathrm{I}}\left(\hat{u}^l_{\mathrm{t,I},j,k}, \hat{v}^l_{\mathrm{t,I},j,k}\right)\right) \mathbf{H}^*_{\mathrm{B2I},j} \mathbf{w}^*_{d,j,i} \right|^2. \tag{46}$$

The optimization problem (P3-1) is still non-convex. Omitting these constraints leads to the following relaxation:

$$\text{(P3-2)}: \min_{\mathbf{V}_j} \max_k \; -\varrho f^{\mathrm{w}}_{1,j,k} + f^{\mathrm{w}}_{2,j,k} + f^{\mathrm{w}}_{3,j,k} + f^{\mathrm{w}}_{4,j,k}, \tag{47a}$$

$$\text{s.t.} \quad (31c), \tag{47b}$$

The above problem can be efficiently solved as SQP. However, the corresponding rank-one solution can be obtained by Gaussian Randomization method [40]. Specifically, let $\mathbf{V}^*_j$ denote the non-rank-one solution, and suppose that the eigenvalue decomposition of $\mathbf{V}^*_j$ is $\mathbf{U\Sigma U}^H$. Then, we set $\tilde{\mathbf{v}} = \mathbf{U\Sigma t}$, where $\mathbf{t} \sim \mathcal{CN}(0, \mathbf{I})$. Ultimately, we can construct a feasible solution $[\mathbf{v}^*]_n = \frac{[\tilde{\mathbf{v}}^*]_n}{|[\tilde{\mathbf{v}}^*]_n|}$.

Finally, by solving the optimization problems (P2-1) and (P3-1) alternately, the beamforming algorithm is guaranteed to converge [37], [38], [39]. And the complexity is $\mathcal{O}\left\{I\left(KN_B^{3.5} + M^{3.5}\right)\right\}$ where I represents the maximum number of required iterations.

B. Downlink Symbol Demodulation and Effective AoAs Estimation

In this subsection, we estimate the transmit signals from the BS and the effective AoAs at the k-th user. Noting that the form of the received signal is similar to the first stage, we can utilize the two proposed algorithms for signal demodulation and AoA estimation.

More specifically, we define $\mathbf{A}^{\mathrm{d}}_{0,j,k} = [\mathbf{H}_{\mathrm{I2U},j,k} \mathbf{\Theta}_j \mathbf{H}_{\mathrm{B2I},j} \mathbf{w}_{\mathrm{d},j,1}, \cdots, \mathbf{H}_{\mathrm{I2U},j,k} \mathbf{\Theta}_j \mathbf{H}_{\mathrm{B2I},j} \mathbf{w}_{\mathrm{d},j,K}] \in C^{N_U \times K}$, $\mathbf{S}_{\mathrm{d},j} = \left[\mathbf{s}^T_{\mathrm{d},j,1}, \cdots, \mathbf{s}^T_{\mathrm{d},j,K}\right]^T \in \mathbb{C}^{K \times T_j}$, $\mathbf{Y}_{\mathrm{d},j,k} = [\mathbf{y}_{\mathrm{d},j,k}(1), \cdots, \mathbf{y}_{\mathrm{d},j,k}(T_j)]$, and $\mathbf{N}_{\mathrm{d}} = [\mathbf{n}_{\mathrm{d}}(1), \cdots, \mathbf{n}_{\mathrm{d}}(T_j)] \in \mathbb{C}^{N_U \times T_j}$, and the received signal from BS to the k-th user during the time block j can be written as

$$\mathbf{Y}_{\mathrm{d},j,k} = \mathbf{A}^{\mathrm{d}}_{0,j,k} \mathbf{S}_{\mathrm{d},j} + \mathbf{N}_{\mathrm{d}}, j = 1, 2, \tag{48}$$

which is also a linear mixture with respect to the transmitted signal, the linear mixing matrix and the signal can be estimated using the BSE-SD algorithm. Then, we are going to estimate the AoAs at the user by the E-angle algorithm.[8] Recall (8),

$$\begin{aligned} \left[\mathbf{A}^{\mathrm{d}}_{0,j,k}\right]_{(m,:)} &= \mathbf{H}_{\mathrm{I2U},j,k} \mathbf{\Theta}_j \mathbf{H}_{\mathrm{B2I},j} \mathbf{w}_{\mathrm{d},j,m} \\ &= \sum_{l=1}^{L_{\mathrm{I2U},j,k}} \alpha^l_{\mathrm{I2U},j,k} \mathbf{a}_{\mathrm{U}}\left(u^l_{\mathrm{r,U},j,k}, v^l_{\mathrm{r,U},j,k}\right) \mathbf{a}^{\mathrm{H}}_{\mathrm{I}}\left(u^l_{\mathrm{t,I},j,k}, v^l_{\mathrm{t,I},j,k}\right) \mathbf{\Theta}_j \mathbf{H}_{\mathrm{B2I},j} \mathbf{w}_{\mathrm{d},j,m} \\ &= \mathbf{B}^{\mathrm{d}}_{\mathrm{I},j,k} \mathbf{e}^{\mathrm{d}}_{\mathrm{U},j,k,m}, \end{aligned} \tag{49}$$

where

$$\mathbf{B}^{\mathrm{d}}_{\mathrm{U},j,k} = \left[\mathbf{a}_{\mathrm{U}}\left(u^1_{\mathrm{r,U},j,k}, v^1_{\mathrm{r,U},j,k}\right), \cdots, \mathbf{a}_{\mathrm{U}}\left(u^{L_{\mathrm{I2U},j,k}}_{\mathrm{r,U},j,k}, v^{L_{\mathrm{I2U},j,k}}_{\mathrm{r,U},j,k}\right)\right], \tag{50}$$

and

$$\mathbf{e}^{\mathrm{u}}_{\mathrm{U},j,k,m} = [\beta^1_{\mathrm{t,I},j,k}, \cdots, \beta^{L_{\mathrm{I2U},j,k,m}}_{\mathrm{t,I},j,k,m}], \tag{51}$$

where $\beta^l_{\mathrm{t,I},j,k,m} = \alpha^l_{\mathrm{I2U},j,k} \mathbf{a}^{\mathrm{H}}_{\mathrm{I}}\left(u^l_{\mathrm{t,I},j,k}, v^l_{\mathrm{t,I},j,k}\right) \mathbf{\Theta}_j \mathbf{H}_{\mathrm{B2I},j} \mathbf{w}_{\mathrm{d},j,m}$.

Let $\hat{\mathbf{A}}^{\mathrm{d}}_{2,j,k}$ and $\hat{\mathbf{s}}_{\mathrm{d}2,j,k}$ denote the estimated linear mixing matrix and the signal transmitted to the k-th user. Then, we estimate the effective AoAs from the j-th sub-IRS to the k-th user using the E-angle algorithm. However, different from the user access stage, each column of $\mathbf{A}^{\mathrm{d}}_{0,j,k}$ contains the channel from the BS to the j-th sub-IRS and then to the k-th user. Thus, the input in the E-angle algorithm is $\mathbf{A}^{\mathrm{d}}_{0,j,k}$ and the auto-correlation matrix used in the FBSS process can be estimated by

$$\hat{\mathbf{R}}^{\mathrm{d}}_{1,j,k} = \frac{1}{2KN_{\mathrm{m},j}} \sum_{m=1}^{N_{\mathrm{m},j}} \sum_{k=1}^{K} \left\{ \left[\hat{\mathbf{A}}^{\mathrm{d}}_{2,j,k}\right]_{(:,k),m} \left(\left[\hat{\mathbf{A}}^{\mathrm{d}}_{2,j,k}\right]_{(:,k),m} \right)^H \right.$$

[8] It can be observed that compared to the linear mixing matrix during the first stage, i.e., $\mathbf{A}^{\mathrm{u}}_{0,j}$, each column of the linear mixing matrix $\mathbf{A}^{\mathrm{d}}_{0,j,k}$ can be written as the product of the array response at the k-th user and the beamforming vector. Consequently, it provides a higher degree of freedom (K times) and yields superior performance. Moreover, we consider exploiting the estimated AoAs during the second stage for channel estimation and localization, during which the semi-passive reflecting elements are operated in the reflecting mode, thus the accuracy of angle estimation at the user side is independent of M_a.

$$+\mathbf{J}\left(\left[\hat{\mathbf{A}}^{\mathrm{d}}_{2,j,k}\right]_{(:,k),m}\right)^{*}\left(\left[\hat{\mathbf{A}}^{\mathrm{d}}_{2,j,k}\right]_{(:,k),m}\right)^{T}\mathbf{J}\Bigg\}, \tag{52}$$

based on which, the effective AoAs from the j-th sub-IRS to the k-th user can be estimated as $\{\hat{u}^{l}_{\mathrm{r,U},j,k},\hat{v}^{l}_{\mathrm{r,U},j,k}\}, l = 1,\cdots,L_{\mathrm{I2U},j,k}$.

C. Channel Reconstruction

According to the angular reciprocity between downlink and uplink channels, the linear mixing matrix and the effective AoAs estimated in both the user stage and the downlink transmission stage can be exploited to reconstruct the channel between the j-th sub-IRS and the k-th user. However, the ambiguity of the complex gain and the mismatch of effective AoA pairs in both uplink and downlink transmission should be eliminated, which is performed as follows:

Firstly, determine the AoA pairs corresponding to the links between the j-th sub-IRS and the k-th user, we define

$$\hat{\mathbf{B}}^{\mathrm{u}}_{\mathrm{I},j,k} = \left[\mathbf{a}_{\mathrm{I}}\left(\hat{u}^{1}_{\mathrm{r,I},j,k},\hat{v}^{1}_{\mathrm{r,I},j,k}\right),\cdots,\mathbf{a}_{\mathrm{I}}\left(\hat{u}^{L_{\mathrm{I2U},j,k}}_{\mathrm{r,I},j,k},\hat{v}^{L_{\mathrm{I2U},j,k}}_{\mathrm{r,I},j,k}\right)\right], \tag{53}$$

and calculate

$$\begin{aligned}\hat{\mathbf{e}}^{\mathrm{u}}_{\mathrm{U},j,k} &= \left(\hat{\mathbf{B}}^{\mathrm{u}}_{\mathrm{I},j,k}\right)^{\dagger}\left[\hat{\mathbf{A}}^{\mathrm{u}}_{2,j}\right]_{(k,:)} \\ &= [\hat{\alpha}^{1}_{\mathrm{I2U},j,k}\mathbf{a}^{\mathrm{H}}_{\mathrm{U}}\left(\hat{u}^{1}_{\mathrm{t,U},j,1},\hat{v}^{1}_{\mathrm{t,U},j,1}\right)\mathbf{w}_{\mathrm{u},k}, \\ &\quad \cdots,\hat{\alpha}^{L_{\mathrm{I2U},j,k}}_{\mathrm{I2U},j,k}\mathbf{a}^{\mathrm{H}}_{\mathrm{U}}\left(\hat{u}^{L_{\mathrm{I2U},j,k}}_{\mathrm{t,U},j,K},\hat{v}^{L_{\mathrm{I2U},j,k}}_{\mathrm{t,U},j,k}\right)\mathbf{w}_{\mathrm{u},k}]^{T}.\end{aligned} \tag{54}$$

In order to eliminate the mismatch of effective AoA pairs, $\left(\hat{\mathbf{c}}^{\mathrm{d}}_{\mathrm{U},j,k}\right)_{m}, m \in \{1,\cdots,L_{\mathrm{I2U},j,k}!\}$, which contains all the possible sequences of the effective AoAs from the j-th sub-IRS to the k-th user, i.e., $(\hat{u}^{l}_{\mathrm{r,U},j,k},\hat{v}^{l}_{\mathrm{r,U},j,k}), l = \{1,\cdots,L_{\mathrm{I2U},j,k}\}$, are constructed, for example

$$\begin{aligned}\left(\hat{\mathbf{c}}^{\mathrm{d}}_{\mathrm{U},j,k}\right)_{L_{\mathrm{I2U},j,k}!} = \Big[&\mathbf{a}_{\mathrm{U}}\left(\hat{u}^{L_{\mathrm{I2U},j,k}}_{\mathrm{r,U},j,k},\hat{v}^{L_{\mathrm{I2U},j,k}}_{\mathrm{r,U},j,k}\right)\mathbf{w}_{\mathrm{u},k} \\ &\cdots,\mathbf{a}_{\mathrm{U}}\left(\hat{u}^{1}_{\mathrm{r,U},j,k},\hat{v}^{1}_{\mathrm{r,U},j,k}\right)\mathbf{w}_{\mathrm{u},k},\Big].\end{aligned} \tag{55}$$

The correct order corresponding to $(\hat{u}^{1}_{\mathrm{r,I},j,k},\hat{v}^{1}_{\mathrm{r,I},j,k})$ can be matched as

$$\hat{\mathbf{e}}^{\mathrm{d}}_{\mathrm{U},j,k} = \left(\hat{\mathbf{c}}^{\mathrm{d}}_{\mathrm{U},j,k}\right)_{m}, \tag{56}$$

where

$$m = \arg\min_{m}\left\{\mathrm{Seq}\left[\left|\left(\hat{\mathbf{c}}^{\mathrm{d}}_{\mathrm{U},j,k}\right)_{m}\right|_{\mathrm{des}}\right] - \mathrm{Seq}\left[\left|\hat{\mathbf{e}}^{\mathrm{u}}_{\mathrm{U},j,k}\right|_{\mathrm{des}}\right]\right\}, \tag{57}$$

and $\mathrm{Seq}\left[\left|\hat{\mathbf{e}}^{\mathrm{u}}_{\mathrm{U},j,k}\right|_{\mathrm{des}}\right]$ denotes the index corresponding to the elements of $\hat{\mathbf{e}}^{\mathrm{u}}_{\mathrm{U},j,k}$ that are sorted in a descending order.

Then, the complex gain corresponding to each pair of effective AoAs can be estimated by

$$\hat{\alpha}^{l}_{\mathrm{I2U},j,k} = \frac{[\hat{\mathbf{e}}^{\mathrm{u}}_{\mathrm{U},j,k}]_{l}}{\hat{\mathbf{e}}^{\mathrm{d}}_{\mathrm{U},j,k}}, l = 1,\cdots,L_{\mathrm{I2U},j,k}. \tag{58}$$

Finally, we reconstruct the channel $\mathbf{H}_{\mathrm{I2U},j,k}$ by

$$\begin{aligned}\hat{\mathbf{H}}_{\mathrm{I2U},j,k} = \sum_{l=1}^{L_{\mathrm{I2U},j,k}}&\hat{\alpha}^{l}_{\mathrm{I2U},j,k}\mathbf{a}_{\mathrm{U}}\left(\hat{u}^{l}_{\mathrm{r,U},j,k},\hat{v}^{l}_{\mathrm{r,U},j,k}\right) \\ &\mathbf{a}^{\mathrm{H}}_{\mathrm{I}}\left(-\hat{u}^{l}_{\mathrm{r,I},j,k},-\hat{v}^{l}_{\mathrm{r,I},j,k}\right).\end{aligned} \tag{59}$$

D. User Location Estimation

In this subsection, the user location is estimated based on the estimated effective AoAs corresponding to the LoS path, i.e., $\{\hat{u}^{l_{\mathrm{LoS}}}_{\mathrm{r,I},j,k},\hat{v}^{l_{\mathrm{LoS}}}_{\mathrm{r,I},j,k}\}$, and $\{\hat{u}^{l_{\mathrm{LoS}}}_{\mathrm{r,U},j,k},\hat{v}^{l_{\mathrm{LoS}}}_{\mathrm{r,U},j,k}\}$, where l_{LoS} is obtained according to the channel reciprocity

$$l_{\mathrm{LoS}} = \arg\min_{l,p}\left\{\hat{v}^{l}_{\mathrm{r,U},j,k} + \hat{u}^{p}_{\mathrm{r,I},j,k}, l,p = 1,\cdots,L_{\mathrm{I2U},j,k}\right\}. \tag{60}$$

Let $\mathbf{p}_{\mathrm{I},j} = (x_{\mathrm{I},j},y_{\mathrm{I},j},z_{\mathrm{I},j})^{T}$ and $\hat{\mathbf{p}}_{\mathrm{u},k} = (\hat{x}_{\mathrm{u},k},\hat{y}_{\mathrm{u},k},\hat{z}_{\mathrm{u},k})^{T}$ denote the location of the j-th sub-IRS and the k-th estimated user, respectively, the relationship among the location of the j-th sub-IRS, the position of the k-th user, and the LoS (l_{LoS}) path are given as follows [22], [23]

$$\hat{u}^{l_{\mathrm{LoS}}}_{\mathrm{r,U},j,k} = \frac{\hat{x}_{\mathrm{u},k}-x_{\mathrm{I},j}}{\|\hat{\mathbf{p}}_{\mathrm{u},k}-\mathbf{p}_{\mathrm{I},j}\|}, \hat{v}^{l_{\mathrm{LoS}}}_{\mathrm{r,U},j,k} = \frac{\hat{y}_{\mathrm{u},k}-y_{\mathrm{I},j}}{\|\hat{\mathbf{p}}_{\mathrm{u},k}-\mathbf{p}_{\mathrm{I},j}\|}, j = 1,2. \tag{61}$$

Therefore, denote $\hat{\mathbf{z}}_{k} \triangleq \big(\hat{x}_{\mathrm{u},k},\hat{y}_{\mathrm{u},k},\|\hat{\mathbf{p}}_{\mathrm{u},k}-\mathbf{p}_{\mathrm{I},1}\|, \|\hat{\mathbf{p}}_{\mathrm{u},k}-\mathbf{p}_{\mathrm{I},2}\|\big)^{T}$, which can be obtained by

$$\hat{\mathbf{z}}_{k} = {\mathbf{L}_{k}}^{-1}\mathbf{f}, \tag{62}$$

where

$$\mathbf{L}_{k} \triangleq \begin{pmatrix} 1 & 0 & -\hat{u}^{l_{\mathrm{LoS}}}_{\mathrm{r,U},1,k} & 0 \\ 0 & 1 & -\hat{v}^{l_{\mathrm{LoS}}}_{\mathrm{r,U},1,k} & 0 \\ 1 & 0 & 0 & -\hat{u}^{l_{\mathrm{LoS}}}_{\mathrm{r,U},2,k} \\ 0 & 1 & 0 & -\hat{u}^{l_{\mathrm{LoS}}}_{\mathrm{r,U},2,k} \end{pmatrix}, \tag{63}$$

and

$$\mathbf{f} \triangleq (x_{\mathrm{I},1},y_{\mathrm{I},1},x_{\mathrm{I},2},y_{\mathrm{I},2})^{T}. \tag{64}$$

Besides, $\hat{z}_{\mathrm{u},k}$ can be estimated by

$$\hat{z}_{\mathrm{u},k} = \arg\min_{\omega_{1,k}}\min_{\omega_{1,k}\in\{z_{\mathrm{I},1}\pm d_{\mathrm{z},1,k}\},\omega_{2,k}\in\{z_{\mathrm{I},2}\pm d_{\mathrm{z},2,k}\}}|\omega_{1}-\omega_{2}|, \tag{65}$$

where

$$d_{\mathrm{z},j,k} \triangleq \sqrt{\left(\|\hat{\mathbf{p}}_{\mathrm{u},k}-\mathbf{p}_{\mathrm{I},j}\|^{2}\right)^{2} - (\hat{x}_{\mathrm{u},k}-z_{\mathrm{I},j})^{2} - (\hat{y}_{\mathrm{u},k}-y_{\mathrm{I},j})^{2}}. \tag{66}$$

Combining (62) and (65), we obtain the location of the k-th user $\hat{\mathbf{p}}_{\mathrm{u},k}$.

E. Overall Algorithm and Complexity

The proposed overall two-stage algorithm is summarized in **Algorithm 3**. The primary source of complexity is the computation of the beamforming design scheme, which is $\mathcal{O}\left\{I\left(KN_{B}^{3.5}+M^{3.5}\right)\right\}$, and the eigenvalue decomposition in two stages, which is $\mathcal{O}\left\{M^{2}\tau_{0}+N_{U}^{2}T_{j}+N_{U}^{3}\right\}$. Therefore, the overall complexity is $\mathcal{O}\left\{M^{2}\tau_{0}+N_{U}^{2}T_{j}+N_{U}^{3}+I\left(KN_{B}^{3.5}+M^{3.5}\right)\right\}$.

Algorithm 3 The Two-Stage Algorithm

Stage I: The user access stage
  Input the received signals at the j-th sub-IRS $\mathbf{Y}_{\mathrm{u},j}$
  Estimate the transmit signals $\hat{\mathbf{S}}_{\mathrm{u2}}$ and the mixing matrix $\hat{\mathbf{A}}^{\mathrm{u}}_{2,j}$ by the BSE-SD algorithm.
  Estimate the effective AoAs at the j-th sub-IRS $\{\hat{u}^l_{\mathrm{r,I},j,k}, \hat{v}^l_{\mathrm{r,I},j,k}\}$ by the E-angle algorithm.
Design the joint beamforming based on the effective AoAs at sub-IRSs.
Stage II: The downlink transmission stage
  Input the received signals at the k-th user $\mathbf{Y}_{\mathrm{d},j,k}$.
  Estimate the transmit signals $\hat{\mathbf{s}}_{\mathrm{d2},j,k}$ and the mixing matrix $\hat{\mathbf{A}}^{\mathrm{d}}_{2,j,k}$ by the BSE-SD algorithm, and the AoAs at the k-th user $\{\hat{u}^l_{\mathrm{r,U},j,k}, \hat{v}^l_{\mathrm{r,U},j,k}\}$ by the E-angle algorithm.
  Eliminate the mismatch of the AoA pairs by (53) $\sim$ (57), and estimate the complex gain by (58).
  Reconstruct the channle between the j-th sub-IRS and the k-th user by (59).
  Perform localization by (61) and (64).
Output the estimation of the transmit data $\hat{\mathbf{s}}_{\mathrm{d2},j,k}$, the channel $\hat{\mathbf{H}}_{\mathrm{I2U},j,k}$ and the location of the k-th user $\hat{\mathbf{p}}_{\mathrm{u},k}$.

V. Extension of the Proposed Framework to the Case With Dircet Link

The proposed ISAC framework can be easily extended to the case that the direct link exists between the BS and the users. We can achieve both communication and localization tasks directly using the proposed algorithm and framework by scheduling the BS and IRS on different time blocks. Specifically, using only one IRS is enough to assist the localization and communication. Firstly, turn off the IRS, and the received signal at the BS during the user access stage and the signal at the k-th user during the downlink transmission stage are respectively given by

$$\mathbf{y}_{\mathrm{u,B}}(t) = \sum_{k=1}^{K} \sqrt{P_{\mathrm{u}}}\mathbf{H}_{\mathrm{U2B},k}\mathbf{w}_{\mathrm{u},k}s_{\mathrm{u},k}(t) + \mathbf{n}_{\mathrm{u}}(t), \tag{67}$$

$$\mathbf{y}_{\mathrm{d},k}(t) = \mathbf{H}_{\mathrm{B2U},k}\sum_{i=1}^{K} \mathbf{w}_{\mathrm{d},i}s_{\mathrm{d},i}(t) + \mathbf{n}_{\mathrm{d}}(t), \tag{68}$$

where $\mathbf{H}_{\mathrm{U2B},k}$ denotes the direct link between the BS and the user. The BS and the user can directly use the proposed algorithm to obtain the angle information of the direct link, i.e., $\{\hat{u}^l_{\mathrm{r,B},k}, \hat{u}^l_{\mathrm{r,U},k}\}$, demodulate the transmit signal, and reconstruct the direct channel, respectively. Then, turn on the IRS, the received signal at the IRS during the user access stage and the signal at the k-th user during the downlink transmission stage are respectively given by

$$\mathbf{y}_{\mathrm{u}}(t) = \sum_{k=1}^{K} \sqrt{P_{\mathrm{u}}}\mathbf{H}_{\mathrm{U2I},j,k}\mathbf{w}_{\mathrm{u},k}s_{\mathrm{u},k}(t) + \mathbf{n}_{\mathrm{u}}(t), \tag{69}$$

$$\mathbf{y}_{\mathrm{d},k}(t) = (\mathbf{H}_{\mathrm{B2U},k} + \mathbf{H}_{\mathrm{I2U},k}\mathbf{\Theta}\mathbf{H}_{\mathrm{B2I}})\sum_{i=1}^{K} \mathbf{w}_{\mathrm{d},i}s_{\mathrm{d},i}(t) + \mathbf{n}_{\mathrm{d}}(t). \tag{70}$$

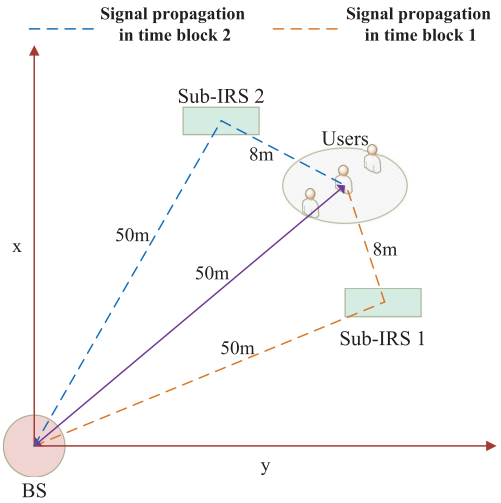

Fig. 5. Simulation setup.

And the proposed algorithm can be directly utilized to demodulate the transmit signal and reconstruct the effective channel, i.e., $(\mathbf{H}_{\mathrm{B2U},k} + \mathbf{H}_{\mathrm{I2U},k}\mathbf{\Theta}\mathbf{H}_{\mathrm{B2I}})$. By using successive interference cancellation (SIC) method, the cascaded channel can be reconstructed. Then, the proposed algorithm can be utilized to distinguish the LoS path of the direct and cascaded channel, and the location can be estimated.

VI. Numerical Results

In this section, we provide simulation results to demonstrate the effectiveness of the proposed I-CALL framework, the communication and localization performance of the proposed algorithm and draw valuable insights.

A. Simulation Setup

The simulation setup is shown in Fig. 5, where the BS is 10 meters above the horizontal floor, $K = 3$ users are 2 meters, 0 meters, and 2 meters, above the horizontal floor, while the two sub-IRSs are 5 meters and 4 meters above the horizontal floor, respectively [22]. The distances from the BS to the j-th sub-IRSs, to the center of the user cluster, and from the j-th sub-IRSs to the k-th user are respectively set as $d_{\mathrm{B2I},j} = d_{\mathrm{B2Uc}} = 50$ meters and $d_{\mathrm{I2U},j,k} = 8$ meters. The path loss at the reference distance of 1 m is set as $C_0 = 30$ dB with exponents from the BS to the j-th sub-IRS, and from the j-th sub-IRS to the k-th user set as $\kappa = 2.2$ [41]. Without loss of generality, quadrature phase shift keying (QPSK) modulation is considered in the simulation, and unless otherwise specified, the following setup is used: $P = 10$ dBm, $\varrho = 10^3$, $M = 10 \times 10$, $M_a = 4 \times 4$, $\tau_{0,\mathrm{p}} = 5$, $\tau_{0,\mathrm{p}} = 20$, $\tau_1 = 4$, $\tau_2 = 1000$, $N_{\mathrm{m},j} = 4$, $Q_{y,j} = Q_{z,j} = \sqrt{M_a} - 1$, noise power $\sigma^2_{\mathrm{u}} = \sigma^2_{\mathrm{d}} = -110$ dBm, $N_B = N_U = 16$, $L_{\mathrm{B2I},j} = 10$, $L_{\mathrm{I2U},j,k} = 4$, and the angle separation is assumed to be larger than $4/N_B$, $4/M$, and $4/N_U$ at the BS, sub-IRSs, and users [42].

B. Communication Performance

In this subsection, we provide numerical results to verify the communication performance of the proposed system. Firstly,

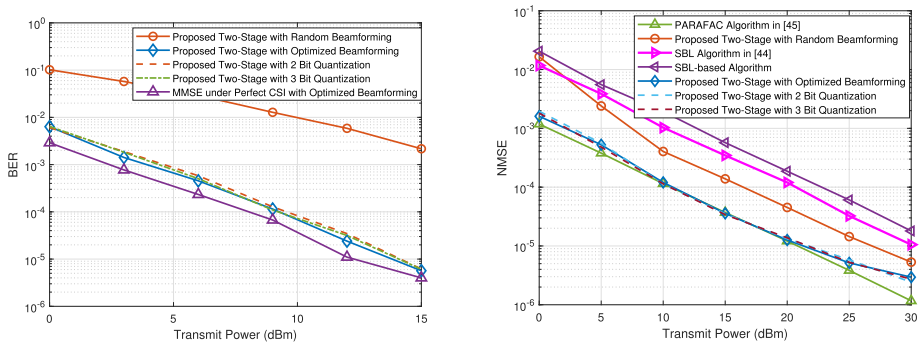

(a) SER of the system. (b) NMSE of the channel estimation.

Fig. 6. The performance of the proposed algorithm compared with the communication-only systems.

we use the normalized mean square error (NMSE) as a metric to evaluate average channel estimation accuracy,

$$\varepsilon_{\mathrm{N}} = \mathbb{E}\left\{ \frac{1}{2K} \sum_{j=1}^{2} \sum_{k=1}^{K} \frac{\left\| \hat{\mathbf{H}}_{\mathrm{I2U},j,k} - \mathbf{H}_{\mathrm{I2U},j,k} \right\|^2}{\left\| \mathbf{H}_{\mathrm{I2U},j,k} \right\|^2} \right\}, \tag{71}$$

and average symbol error rate (SER), i.e.,

$$P_{\mathrm{e}} = \mathbb{E}\left\{ \frac{1}{2K} \sum_{j=1}^{2} \sum_{k=1}^{K} P_{\mathrm{e},k,j} \right\}, \tag{72}$$

as a metric to evaluate signal demodulation performance, where $P_{\mathrm{e},k,j}$ denotes the SER of the k-th user during the j-th time block.

We use two benchmarks to demonstrate the performance of signal demodulation and four benchmarks to demonstrate the performance of channel estimation.

1) Benchmark for Demodulation: Two benchmarks termed the "MMSE under Perfect CSI with Optimized Beamforming" and the "Proposed Two-Stage with Random Beamforming" are given as follows:

a) **MMSE under Perfect CSI with Optimized Beamforming**: The SER is obtained by the classic MMSE method under perfect CSI as in [43] with similar beamforming design scheme as the proposed two-stage algorithm. b) **Proposed Two-Stage with Random Beamforming**: The SER is obtained by the proposed two-stage algorithm but adopts the random beam design at the BS and the sub-IRSs.

2) Benchmark for Channel Estimation: Four benchmarks termed "SBL-based algorithm", "SBL Algorithm in [44]", "Proposed Two-Stage with Random Beamforming", and "PARAFAC Algorithm in [45]", are given as follows with the same pilot sequences as the proposed algorithm:

a) **SBL-based Algorithm**: The channel is estimated by the sparse bayesian learning (SBL) method without grid mismatch, where the angular range is divided into 32 grid points. b) **SBL Algorithm in [44]**: The channel is estimated by the SBL method proposed in [44], considering the transmit beam patterns N_T^{Beam} and receiver beam patterns N_R^{Beam}, where $N_R^{Beam} = N_T^{Beam} = 16$. The angular range is divided into 32 grid points, where the grid mismatch is not considered. c) **Proposed Two-Stage with Random Beamforming**: The channel are estimated by the proposed two-stage algorithm but with random beamforming design both at the BS and at the sub-IRSs. d) **PARAFAC Algorithm in [45]**: The channel are estimated by the parallel factor decomposition (PARAFAC) method as in [45], where the channel between the BS and the sub-IRS $\mathbf{H}_{\mathrm{B2I},j}$ is known as the prior information to eliminate the scaling ambiguities.

Fig. 6 compares the communication performance with other benchmark algorithms, where Fig. 6(a) and Fig. 6(b) show the impact of transmit power on P_{e} and on NMSE, respectively. It is observed in Fig. 6(a) that the average SER of the proposed algorithm decreases with the increase of transmit power. Although the proposed two-stage algorithm is designed for scenarios where CSI is unknown, the average SER of the proposed algorithm is comparable to the MMSE method with perfect CSI, which outperforms the benchmark using random beam design scheme. This validates the effectiveness of the proposed beamforming design algorithm. Fig. 6(b) shows that the estimation accuracy improves with the increase of transmit power. Moreover, the discrete phase shifting coefficients are obtained by quantizing the continuous coherent phase shifting coefficients to its nearest discrete phase level as in [48] for passive beamforming design. Specifically, let b be the number of quantization bits thus the number of phase levels is 2^b and the discrete phase levels can be expressed as $\mathcal{F} = \left\{0, \frac{2\pi}{2^b}, 2\frac{2\pi}{2^b}, \ldots, \left(2^b - 1\right)\frac{2\pi}{2^b}\right\}$. From the figure, it can be observed that 3-bit quantization achieves comparable demodulation and channel estimation accuracy. The channel estimation performance of the proposed algorithm outperforms those of the SBL-based algorithm and the random beamforming scheme since the proposed algorithm exploits the statistical characteristics of the received signal. It is worth noting that the proposed algorithm performs slightly worse than the PARAFAC algorithm. This can be attributed to the fact that PARAFAC assumes perfect CSI between BS and all the sub-IRSs as prior information to eliminate the scaling ambiguities [45], while the proposed algorithm does not require information about CSI. Furthermore, it is worth highlighting that the proposed I-CALL framework offers dual benefits. While its communication performance is comparable to communication-only schemes, it concurrently enables localization capabilities, as demonstrated in Section VI-C.

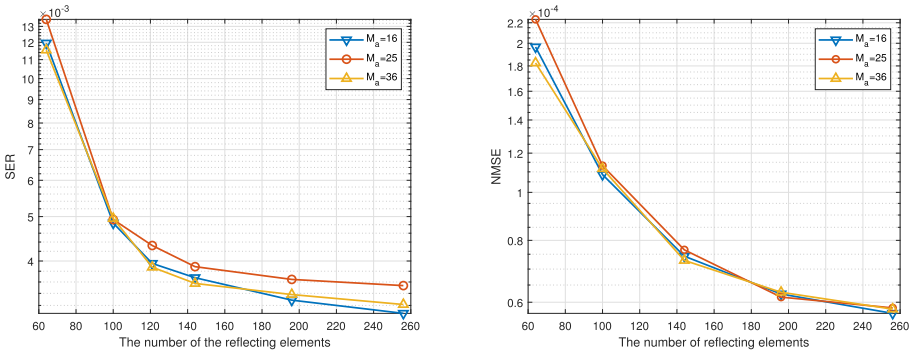

(a) SER of the system. (b) NMSE of the channel estimation.

Fig. 7. Impact of the number of the reflecting elements on the communication performance.

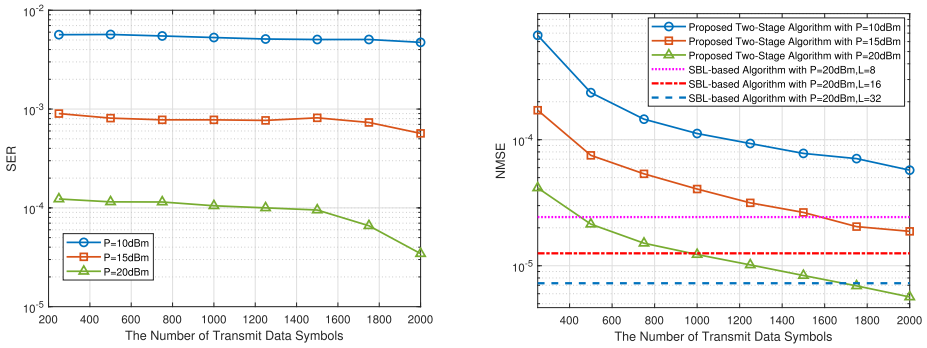

(a) SER of the system. (b) NMSE of the channel estimation.

Fig. 8. Impact of the number of the transmit data symbols on the communication performance.

Fig. 7 shows the impact of the number of the reflecting elements M on the communication performance with $P = 0$ dBm. It can be observed that by increasing M, the average SER and NMSE can be effectively reduced. Specifically, when the number of reflecting elements increases from 64 to 256, the SER is reduced by 71%, and NMSE is reduced by 73%. Nonetheless, due to limited accuracy of CSI obtained in the user access stage, it is observed that both NMSE and SER settles as M grows large. In addition, the impact of the number of semi-passive reflecting elements M_a on the communication performance is also shown in Fig. 7. Numerical results demonstrate that increasing the number of semi-passive elements has a marginal impact on overall communication performance since only partial knowledge of the angle information is considered and the angle of arrival information at the users is unknown. Consequently, the beamforming design scheme cannot eliminate all the inter-user interference, which becomes the major bottleneck of the system performance. As a result, the number of reflecting elements has limited impact on the system performance. This suggests that the deployment of a limited number of semi-passive elements is sufficient to achieve satisfactory communication performance.

Fig. 8 illustrates the communication performance in the downlink transmission stage. It can be observed that increasing the number of transmit data can notably enhance the channel estimation performance. For example, when $P = 20$ dBm, increasing the transmitted data symbols from 250 to 1000 results in a 69.74% enhancement in estimation accuracy. Additionally, we evaluated the channel estimation accuracy of the SBL algorithm with $L = 8$, 16, and 32 pilot symbols. The results show that when the data symbol length is 1000, the proposed method achieves estimation accuracy comparable to that of the SBL algorithm, but with a reduction of 3 pilot symbols. Moreover, when the number of transmitted symbols is increased to 1700, our method achieves more pilot overhead reduction (from 32 to 13 pilot symbols).[9] However, the effect is insignificant on SER in the low transmit power region, but becomes more pronounced with high transmit power. Nevertheless, it is still necessary to increase the number of the transmitted data, with the purpose of obtaining more accurate CSI for subsequent transmissions. The observation also implies that the performance corresponding to high transmit power can be achieved via an increased volume of transmit data, resulting in a reduction in the overall power consumption of the system. This is due to the fact that the BSE-BD algorithm essentially utilizes the higher-order statistical properties of the received signals. Increasing the amount of transmitted data improves the accuracy of statistical characteristics, thereby enhancing communication performance.

[9]In mmWave frequency bands, the coherence time interval may include thousands of modulated symbol times/durations, depending on the carrier frequency, mobile station velocity, and bandwidth [42]. Hence, a large number of transmit data symbols can be utilized to reduce pilot overhead.

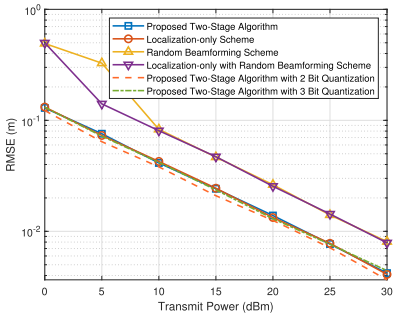

Fig. 9. The localization accuracy of the proposed algorithm compared with the localization-only systems.

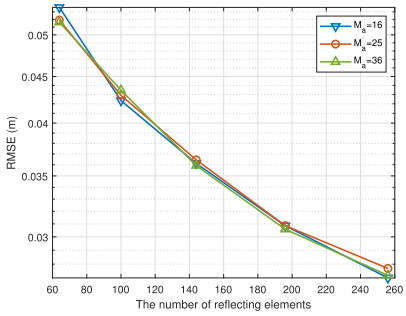

Fig. 10. Impact of the number of the reflecting elements on the localization accuracy.

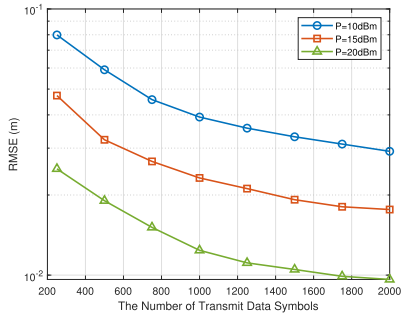

Fig. 11. Impact of the number of the transmit data symbols on the localization accuracy.

C. Localization Performance

In this subsection, we adopt the average root mean square error (RMSE) of the estimated user location as the performance metric,

$$\varepsilon_{\mathrm{R}} = \mathbb{E}\left\{\sqrt{\frac{1}{K}\sum_{k=1}^{K}\|\hat{\mathbf{p}}_{\mathrm{u},k} - \mathbf{p}_{\mathrm{u},k}\|^2}\right\}. \tag{73}$$

We use three benchmarks, termed "Localization-only with Optimized Beamforming","Localization-only with Random Beamforming", and "Proposed Two-Stage with Random Beamforming", to demonstrate the performance of localization accuracy. a) **Localization-only with Optimized Beamforming**: User locations are obtained by TLS-ESPRIT method using localization orthogonal reference signals with the proposed beamforming design scheme. b) **Localization-only with Random Beamforming**: User locations are obtained by TLS-ESPRIT method using localization orthogonal reference signals but with the random beamforming design scheme. c) **Proposed Two-Stage with Random Beamforming**: User locations are obtained by the proposed two-stage algorithm but with the random beam design scheme.

Fig. 9 compares the localization accuracy of the proposed algorithm with the benchmark using a dedicated localization reference signal with a length of $\tau_1 + \tau_2$. It can be observed that the localization accuracy improves with the increase of transmit power, and the proposed two-stage scheme achieves comparable performance to the localization-only scheme, which demonstrates the effectiveness of using the statistical characteristics of the received signal for localization. Specifically, it achieves centimetre-level localization accuracy even with 2-bit and 3-bit quantization.

Fig. 10 shows the impact of the number of IRS reflecting elements on the localization accuracy with $P = 10$ dBm. It is observed that the localization accuracy improves as M increases. Specifically, the localization accuracy increases by 50% with the number of reflecting elements increasing from 64 to 256. In addition, the number of semi-passive elements has little impact on localization accuracy. This outcome aligns with expectations since location estimation relies on effective AoAs at users that are independent of the number of semi-passive reflecting elements.

Fig. 11 illustrates the localization accuracy in the downlink transmission stage, and it is observed that the localization accuracy increases with the number of the data. Although RMSE decreases as the data number increases, this process is hampered by inter-user interference, which has negative impact on the performance of the BSE-BD method. Nevertheless, the localization performance can be improved by increasing the transmit power.

VII. Conclusion

This paper presented the I-CALL framework, a novel approach that capitalizes on semi-passive IRSs for ISAC. The framework enables simultaneous signal demodulation, channel estimation, and localization with reduced pilot overhead. Moreover, we proposed a radar-inspired beamforming scheme to enhance downlink transmission performance. Simulation results demonstrated that the proposed algorithm achieved comparable performance to the communication-only and localization-only systems. It was found that deploying a limited number of semi-passive elements was sufficient to achieve satisfactory performance, resulting in reduced energy consumption. Extending the presented framework to different settings such as multi-cell or cell-free systems remains interesting future directions. Additionally, it's essential to scrutinize this framework under high-mobility conditions, where multipath propagation and temporal channel variations induce doubly-selective channels. These channels, characterized by frequency-selective and time-selective fading, pose significant challenges for achieving reliable location sensing and communication.

References

[1] F. Liu et al., "Integrated sensing and communications: Toward dual-functional wireless networks for 6G and beyond," *IEEE J. Sel. Areas Commun.*, vol. 40, no. 6, pp. 1728–1767, Jun. 2022.

[2] B. Li, A. P. Petropulu, and W. Trappe, "Optimum co-design for spectrum sharing between matrix completion based MIMO radars and a MIMO communication system," *IEEE Trans. Signal Process.*, vol. 64, no. 17, pp. 4562–4575, Sep. 2016.

[3] R. Saruthirathanaworakun, J. M. Peha, and L. M. Correia, "Opportunistic sharing between rotating radar and cellular," *IEEE J. Sel. Areas Commun.*, vol. 30, no. 10, pp. 1900–1910, Nov. 2012.

[4] F. Liu, C. Masouros, A. Li, and T. Ratnarajah, "Robust MIMO beamforming for cellular and radar coexistence," *IEEE Wireless Commun. Lett.*, vol. 6, no. 3, pp. 374–377, Jun. 2017.

[5] L. Zheng, M. Lops, Y. C. Eldar, and X. Wang, "Radar and communication coexistence: An overview: A review of recent methods," *IEEE Signal Process. Mag.*, vol. 36, no. 5, pp. 85–99, Sep. 2019.

[6] S. D. Blunt, P. Yatham, and J. Stiles, "Intrapulse radar-embedded communications," *IEEE Trans. Aerosp. Electron. Syst.*, vol. 46, no. 3, pp. 1185–1200, Jul. 2010.

[7] Q. Wu and R. Zhang, "Towards smart and reconfigurable environment: Intelligent reflecting surface aided wireless network," *IEEE Commun. Mag.*, vol. 58, no. 1, pp. 106–112, Jan. 2020.

[8] C. Xu, B. Clerckx, S. Chen, Y. Mao, and J. Zhang, "Rate-splitting multiple access for multi-antenna joint radar and communications," *IEEE J. Sel. Topics Signal Process.*, vol. 15, no. 6, pp. 1332–1347, Nov. 2021.

[9] F. Liu, Y.-F. Liu, A. Li, C. Masouros, and Y. C. Eldar, "Cramér-rao bound optimization for joint radar-communication beamforming," *IEEE Trans. Signal Process.*, vol. 70, pp. 240–253, 2022.

[10] H. Hua, X. Song, Y. Fang, T. Xiao Han, and J. Xu, "MIMO integrated sensing and communication with extended target: CRB-rate tradeoff," 2022, *arXiv:2205.14050*.

[11] X. Chen, Z. Feng, Z. Wei, P. Zhang, and X. Yuan, "Code-division OFDM joint communication and sensing system for 6G machine-type communication," *IEEE Internet Things J.*, vol. 8, no. 15, pp. 12093–12105, Aug. 2021.

[12] Q. Wu, S. Zhang, B. Zheng, C. You, and R. Zhang, "Intelligent reflecting surface aided wireless communications: A tutorial," *IEEE Trans. Commun.*, vol. 69, no. 5, pp. 3313–3351, May 2021.

[13] Y. Zhang, C. You, and B. Zheng, "Multi-active multi-passive (MAMP)-IRS aided wireless communication: A multi-hop beam routing design," *IEEE J. Sel. Areas Commun.*, vol. 41, no. 8, pp. 2497–2513, Aug. 2023.

[14] Y. Su, X. Pang, S. Chen, X. Jiang, N. Zhao, and F. R. Yu, "Spectrum and energy efficiency optimization in IRS-assisted UAV networks," *IEEE Trans. Commun.*, vol. 70, no. 10, pp. 6489–6502, Oct. 2022.

[15] W. Wei, X. Pang, J. Tang, N. Zhao, X. Wang, and A. Nallanathan, "Secure transmission design for aerial IRS assisted wireless networks," *IEEE Trans. Commun.*, vol. 71, no. 6, pp. 3528–3540, Jun. 2023.

[16] R. S. Prasobh Sankar, S. Prabhakar Chepuri, and Y. C. Eldar, "Beamforming in integrated sensing and communication systems with reconfigurable intelligent surfaces," 2022, *arXiv:2206.07679*.

[17] Z. Xing, R. Wang, and X. Yuan, "Joint active and passive beamforming design for reconfigurable intelligent surface enabled integrated sensing and communication," *IEEE Trans. Commun.*, vol. 71, no. 4, pp. 2457–2474, Apr. 2023.

[18] J. Zuo, Y. Liu, C. Zhu, Y. Zou, D. Zhang, and N. Al-Dhahir, "Exploiting NOMA and RIS in integrated sensing and communication," 2022, *arXiv:2210.02725*.

[19] M. Hua, Q. Wu, C. He, S. Ma, and W. Chen, "Joint active and passive beamforming design for IRS-aided radar-communication," *IEEE Trans. Wireless Commun.*, vol. 22, no. 4, pp. 2278–2294, Apr. 2023.

[20] M. Hua, Q. Wu, W. Chen, O. A. Dobre, and A. Lee Swindlehurst, "Secure intelligent reflecting surface aided integrated sensing and communication," 2022, *arXiv:2207.09095*.

[21] Z. Wang, X. Mu, and Y. Liu, "STARS enabled integrated sensing and communications," *IEEE Trans. Wireless Commun.*, vol. 22, no. 10, pp. 6750–6765, Oct. 2023, doi: 10.1109/TWC.2023.3245297.

[22] Z. Yu, X. Hu, C. Liu, M. Peng, and C. Zhong, "Location sensing and beamforming design for IRS-enabled multi-user ISAC systems," *IEEE Trans. Signal Process.*, vol. 70, pp. 5178–5193, 2022.

[23] X. Hu, C. Liu, M. Peng, and C. Zhong, "IRS-based integrated location sensing and communication for mmWave SIMO systems," *IEEE Trans. Wireless Commun.*, vol. 22, no. 6, pp. 4132–4145, Jun. 2022, doi: 10.1109/TWC.2022.3223428.

[24] A. Taha, M. Alrabeiah, and A. Alkhateeb, "Deep learning for large intelligent surfaces in millimeter wave and massive MIMO systems," in *Proc. IEEE Global Commun. Conf. (GLOBECOM)*, Waikoloa, HI, USA, Dec. 2019, pp. 1–6.

[25] S. Liu, Z. Gao, J. Zhang, M. D. Renzo, and M. Alouini, "Deep denoising neural network assisted compressive channel estimation for mmWave intelligent reflecting surfaces," *IEEE Trans. Veh. Technol.*, vol. 69, no. 8, pp. 9223–9228, Aug. 2020.

[26] A. A. M. Saleh and R. Valenzuela, "A statistical model for indoor multipath propagation," *IEEE J. Sel. Areas Commun.*, vol. JSAC-5, no. 2, pp. 128–137, Feb. 1987.

[27] J. Lee, G.-T. Gil, and Y. H. Lee, "Channel estimation via orthogonal matching pursuit for hybrid MIMO systems in millimeter wave communications," *IEEE Trans. Commun.*, vol. 64, no. 6, pp. 2370–2386, Jun. 2016.

[28] O. E. Ayach, S. Rajagopal, S. Abu-Surra, Z. Pi, and R. W. Heath, "Spatially sparse precoding in millimeter wave MIMO systems," *IEEE Trans. Wireless Commun.*, vol. 13, no. 3, pp. 1499–1513, Mar. 2014.

[29] X. Wei, D. Shen, and L. Dai, "Channel estimation for RIS assisted wireless communications—Part II: An improved solution based on double-structured sparsity," *IEEE Commun. Lett.*, vol. 25, no. 5, pp. 1403–1407, May 2021.

[30] L. Sarperi, X. Zhu, and A. K. Nandi, "Blind OFDM receiver based on independent component analysis for multiple-input multiple-output systems," *IEEE Trans. Wireless Commun.*, vol. 6, no. 11, pp. 4079–4089, Nov. 2007.

[31] J.-F. Cardoso, "High-order contrasts for independent component analysis," *Neural Comput.*, vol. 11, no. 1, pp. 157–192, Jan. 1999.

[32] L. Albera, A. Ferreol, P. Chevalier, and P. Comon, "ICAR: A tool for blind source separation using fourth-order statistics only," *IEEE Trans. Signal Process.*, vol. 53, no. 10, pp. 3633–3643, Oct. 2005.

[33] Y. Jiang, X. Zhu, E. Lim, L. Dong, and Y. Huang, "Low-complexity independent component analysis based semi-blind receiver for wireless multiple-input multiple-output systems," *Int. J. Des., Anal. Tools Integr. Circuits Syst.*, vol. 2, no. 2, pp. 91–98, Aug. 2011.

[34] H. L. Van Trees, *Optimum Array Processing: Part IV of Detection, Estimation, and Modulation Theory*. New York, NY, USA: Wiley, 2004.

[35] J. Li and P. Stoica, "MIMO radar with colocated antennas," *IEEE Signal Process. Mag.*, vol. 24, no. 5, pp. 106–114, Sep. 2007.

[36] P. Stoica, J. Li, and Y. Xie, "On probing signal design for MIMO radar," *IEEE Trans. Signal Process.*, vol. 55, no. 8, pp. 4151–4161, Aug. 2007.

[37] X. Song et al., "Joint transmit and reflective beamforming for IRS-assisted integrated sensing and communication," in *Proc. IEEE Wireless Commun. Netw. Conf. (WCNC)*, Apr. 2022, pp. 189–194.

[38] K.-C. Toh, "An inexact primal–dual path following algorithm for convex quadratic SDP," *Math. Program.*, vol. 112, no. 1, pp. 221–254, Jul. 2007.

[39] X. Liu, T. Huang, N. Shlezinger, Y. Liu, J. Zhou, and Y. C. Eldar, "Joint transmit beamforming for multiuser MIMO communications and MIMO radar," *IEEE Trans. Signal Process.*, vol. 68, pp. 3929–3944, 2020.

[40] Q. Wu and R. Zhang, "Intelligent reflecting surface enhanced wireless network via joint active and passive beamforming," *IEEE Trans. Wireless Commun.*, vol. 18, no. 11, pp. 5394–5409, Nov. 2019.

[41] C. You, B. Zheng, and R. Zhang, "Wireless communication via double IRS: Channel estimation and passive beamforming designs," *IEEE Wireless Commun. Lett.*, vol. 10, no. 2, pp. 431–435, Feb. 2021.

[42] J. He, H. Wymeersch, and M. Juntti, "Channel estimation for RIS-aided mmWave MIMO systems via atomic norm minimization," *IEEE Trans. Wireless Commun.*, vol. 20, no. 9, pp. 5786–5797, Sep. 2021.

[43] Q. Shi, M. Razaviyayn, M. Hong, and Z.-Q. Luo, "SINR constrained beamforming for a MIMO multi-user downlink system: Algorithms and convergence analysis," *IEEE Trans. Signal Process.*, vol. 64, no. 11, pp. 2920–2933, Feb. 2016.

[44] A. Mishra, A. Rajoriya, A. K. Jagannatham, and G. Ascheid, "Sparse Bayesian learning-based channel estimation in millimeter wave hybrid MIMO systems," in *Proc. IEEE 18th Int. Workshop Signal Process. Adv. Wireless Commun. (SPAWC)*, Jul. 2017, pp. 1–5.

[45] G. T. de Araújo, A. L. F. de Almeida, and R. Boyer, "Channel estimation for intelligent reflecting surface assisted MIMO systems: A tensor modeling approach," *IEEE J. Sel. Topics Signal Process.*, vol. 15, no. 3, pp. 789–802, Apr. 2021.

[46] Z.-Q. Luo, W.-K. Ma, A. So, Y. Ye, and S. Zhang, "Semidefinite relaxation of quadratic optimization problems," *IEEE Signal Process. Mag.*, vol. 27, no. 3, pp. 20–34, May 2010.

[47] G. Zhou et al., "A framework of robust transmission design for IRS-aided MISO communications with imperfect cascaded channels," *IEEE Trans. Signal Process.*, vol. 68, pp. 5092–5106, 2020.

[48] Z. Sun and Y. Jing, "On the performance of multi-antenna IRS-assisted NOMA networks with continuous and discrete IRS phase shifting," *IEEE Trans. Wireless Commun.*, vol. 21, no. 5, pp. 3012–3023, May 2022.

[49] S. Kuutti, S. Fallah, K. Katsaros, M. Dianati, F. Mccullough, and A. Mouzakitis, "A survey of the state-of-the-art localization techniques and their potentials for autonomous vehicle applications," *IEEE Internet Things J.*, vol. 5, no. 2, pp. 829–846, Apr. 2018.

[50] Y. Qi, H. Suda, and H. Kobayashi, "On time-of arrival positioning in a multipath environment," in *Proc. IEEE 60th Veh. Technol. Conf.*, Mar. 2004, pp. 3540–3544.

[51] A. J. Weiss, "On the accuracy of a cellular location system based on RSS measurements," *IEEE Trans. Veh. Technol.*, vol. 52, no. 6, pp. 1508–1518, Nov. 2003.

Xingyu Peng (Graduate Student Member, IEEE) received the B.S. degree in information science and engineering from Shandong University, Qingdao, China, in 2021. He is currently pursuing the Ph.D. degree with the Institute of Information and Communication Engineering, Zhejiang University. His research interests include intelligent reflecting surface and integrated sensing, and communication.

Xiaoling Hu (Member, IEEE) received the B.S. degree in electronics and information engineering from Dalian University of Technology, Dalian, China, in 2016, and the Ph.D. degree in information and communication engineering from Zhejiang University, Hangzhou, China, in 2021. She is currently an Associate Professor with Beijing University of Posts and Telecommunications, Beijing, China. Her research interests include reconfigurable intelligent surface (RIS), integrated sensing and communication (ISAC), wireless sensing, and massive MIMO and mmWave. She and her coauthors received the Best Paper Award at IEEE GLOBECOM 2020, IEEE ICC 2019, IEEE ICC 2022, and WCSP 2023.

Jiabao Gao received the B.S. degree in information engineering from Zhejiang University, Hangzhou, China, in 2019, where he is currently pursuing the Ph.D. degree with Zhejiang Provincial Key Laboratory of Information Processing, Communication and Networking. From September 2021 to March 2023, he was a Visiting Student with the Department of Electrical and Electronic Engineering, Imperial College London, U.K. His current research interests include millimeter wave and THz massive MIMO and deep learning for wireless communications.

Richeng Jin (Member, IEEE) received the B.S. degree in information and communication engineering from Zhejiang University, Hangzhou, China, in 2015, and the Ph.D. degree in electrical engineering from North Carolina State University, Raleigh, NC, USA, in 2020. He was a Post-Doctoral Researcher in electrical and computer engineering with North Carolina State University, Raleigh, NC, USA, from 2021 to 2022. He is currently a Faculty Member of the Department of Information and Communication Engineering, Zhejiang University. His research interests are in the general area of wireless AI, game theory, and security and privacy in machine learning/artificial intelligence and wireless networks.

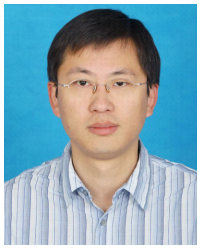

Xiaoming Chen (Senior Member, IEEE) received the B.Sc. degree in electronic engineering from Hohai University in 2005, the M.Sc. degree in electronic engineering from Nanjing University of Science and Technology in 2007, and the Ph.D. degree in electronic engineering from Zhejiang University, Hangzhou, China, in 2011. He is currently a Professor with the College of Information Science and Electronic Engineering, Zhejiang University. From March 2011 to October 2016, he was with Nanjing University of Aeronautics and Astronautics, Nanjing, China. From February 2015 to June 2016, he was a Humboldt Research Fellow with the Institute for Digital Communications, Friedrich-Alexander-University Erlangen-Nürnberg (FAU), Germany. His research interests focus on LEO satellite constellation, the Internet of Things, and smart communications.

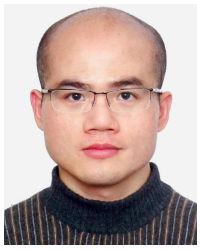

Caijun Zhong (Senior Member, IEEE) received the B.S. degree in information engineering from Xi'an Jiaotong University, Xi'an, China, in 2004, and the M.S. degree in information security and the Ph.D. degree in telecommunications from University College London, London, U.K., in 2006 and 2010, respectively. From September 2009 to September 2011, he was a Research Fellow with the Institute for Electronics, Communications and Information Technologies (ECIT), Queen's University Belfast, Belfast, U.K. Since September 2011, he has been with Zhejiang University, Hangzhou, China, where he is currently a Professor. His current research interests include reconfigurable intelligent surfaces assisted communications and artificial intelligence-based wireless communications. He was a recipient of the 2013 IEEE ComSoc Asia–Pacific Outstanding Young Researcher Award. He and his coauthors received the Best Paper Award at IEEE GLOBECOM 2020 and IEEE ICC 2019. He is an Editor of *Science China Information Science* and *China Communications*. He was an Editor of IEEE TRANSACTIONS ON WIRELESS COMMUNICATIONS and IEEE COMMUNICATIONS LETTERS.